Title
ASSOCIATED PRODUCTION FROM 1.5 TO 2.4 BeV/c

Author
Schwartz, Joseph Adam.

Publication Date
1964-06-29

University of California

Ernest O. Lawrence Radiation Laboratory

ASSOCIATED PRODUCTION FROM 1.5 TO 2.4 BeV/c

Berkeley, California

UCRL-11360

UNIVERSITY OF CALIFORNIA
Lawrence Radiation Laboratory
Berkeley, California

AEC Contract No. W-7405-eng-48

ASSOCIATED PRODUCTION FROM 1.5 TO 2.4 BeV/c

Joseph Adam Schwartz

(Ph. D. Thesis)

June 29, 1964

Printed in USA. Price $1.50. Available from the
Office of Technical Services
U. S. Department of Commerce
Washington 25, D.C.

ASSOCIATED PRODUCTION FROM 1.5 TO 2.4 BeV/c

Contents

ASSOCIATED PRODUCTION FROM 1.5 TO 2.4 BeV/c

Joseph Adam Schwartz

Lawrence Radiation Laboratory
University of California
Berkeley, California

June 29, 1964

ABSTRACT

The two-body final states $\pi p \to \Sigma^0 K^0$, $\pi p \to \Sigma^- K^+$, and $\pi p \to \Lambda K^0$ have studied in the Lawrence Radiation Laboratory 72-inch hydrogen bubble chamber. The cross sections decrease uniformly from 1.5 to 2.4 BeV/c with no evidence for an enhancement from any of the nucleon isobars located in this energy range. The average cross sections are $\sigma(\Sigma^0 K^0) = 115\ \mu b$, $\sigma(\Sigma^- K^+) = 70\ \mu b$, and $\sigma(\Lambda K) = 180\ \mu b$.

The $\Sigma^- K^+$ angular distributions are well described by s and p waves only; $\Sigma^0 K^0$ and ΛK^0 each show evidence for higher partial waves. A simple K*-exchange model fits the data poorly for both $\Sigma^0 K^0$ and ΛK^0. There is evidence for the coupling of $N^*_{1/2}(2190)$ to the ΛK channel but no definite spin assignment can be made, although $G_{7/2}$ is somewhat favored over a $J = 9/2$ assignment. The backward peak in the ΛK angular distribution can be fitted with a form $d\sigma/d\Omega = \sigma_0 e^{At}$ with $A \approx 7\ (\text{BeV}/c)^{-1}$. The values of A obtained in this way are suggestive of the logarithmic shrinking predicted by the Regge-pole analyses of high-energy backward (diffraction) scattering.

I. INTRODUCTION

Numerous authors have reported results on the associated production reactions, $\pi p \rightarrow YK$, at energies from threshold to 1.5 BeV/c.[1-11] This work is an extension of those studies into the energy range 1.5 to 2.4 BeV/c.

All together 240,000 pictures were taken in the Lawrence Radiation Laboratory 72-inch bubble chamber, yielding 11,000 strange-particle interactions. Figure 1 is a histogram of the number of events vs beam momentum, which for constant cross section shows the distribution of path length in the experiment. Thirty-five percent of the events involved the two-body final states, $\pi p \rightarrow \Sigma^- K^+$ (1500 events), $\pi p \rightarrow \Sigma^0 K^0$ (500 events), and $\pi p \rightarrow \Lambda K$ (2000 events). The data are divided into eight beam momentum intervals, so that the statistical errors at any one momentum are roughly 7% for $\Sigma^- K^+$ and ΛK^0 and 15% for $\Sigma^0 K^0$.

In bubble chamber experiments of this type small but cumulative inefficiencies creep in at various stages of the processing, resulting in a net loss of events which must be combatted. The experimental procedures adopted were designed to keep these systematic errors within the stated statistical limits. Section II describes the details of the processing and the major sources of bias.

Section III gives the corrected experimental results and a discussion of possible production mechanisms involved in the formation of these states. In two-body collision processes energy-momentum conservation restricts the number of independent variables to two, which we take to be the beam momentum and center-of-mass production angle. Thus our analysis automatically involves studying the changes in the angular distributions as a function of momentum. When resonances are known to be present this is an effective method of isolating the contribution of the resonant state from a (presumed) slowly varying background. This program has been most successfully exploited by Tripp, Ferro-Luzzi, and Watson[12] in their classic analysis

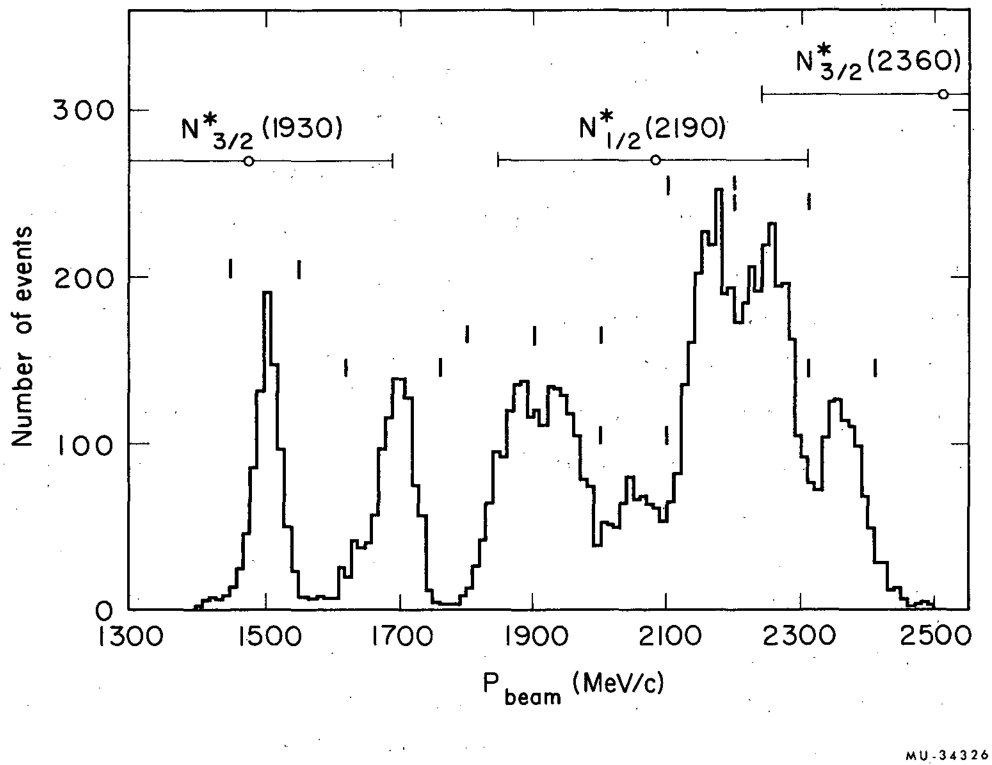

Fig. 1. Histogram of fitted events vs fitted beam momentum for all event types. The vertical marks show the eight beam momentum intervals.

of $Y_0^*(1520)$. The one other popular theme that appears in the analysis of production mechanisms is the peripheral or one-meson-exchange model. The recent theoretical analyses of high-energy scattering in terms of the exchange of Regge poles can be considered as a sort of super peripheralism. I present a discussion of the data terms of both these models.

II. EXPERIMENTAL PROCEDURES

A. Scanning

The scanners were instructed to record all interactions involving strange particles. Frames with too many tracks were skipped but no fiducial volume restriction or other acceptance criteria were imposed. The film was completely scanned twice, and the additional events found in the second scan were re-examined in order to discard nonevents or events failing the cutoffs (Section II. B). There remained 1700 second-scan events to be added to the experiment.

The nominal efficiency obtained by comparing the two scans is 90% for single V's and Σ's and 95% for double V's. The combined efficiency, ϵ_{12}, for all types is greater than 99% ($\epsilon_{12} = \epsilon_1 + \epsilon_2 - \epsilon_1 \epsilon_2$). This assumes that the two scans are independent, which in fact is not true: certain events are systematically missed by both scanners. Σ^- produced in the forward hemisphere at our energies are all minimum-ionizing, so that the decay $\Sigma^- \rightarrow \pi^- + n$ isn't detected for π^- emitted at small angles to the Σ line of flight. Figure 2 is a histogram of the c.m. decay angle of the π^- in Σ decay (should be isotropic if parity is conserved in strong interactions). The suppression of events in the forward direction is quite marked and amounts to about a 5% effect. We correct this slight bias by rejecting all events with $0.8 < \cos\theta_{\pi^-} < 1$ and multiplying the final results by a factor 10/9.

B. Acceptance Criteria and Corrections

There are essentially two different acceptance criteria, each serving somewhat different purposes. The traditional χ^2 tests are a convenient index for choosing between competing hypotheses and for rejecting bad events. Geometrical cutoffs, on the lengths of tracks and the location of the event in the chamber, are imposed mainly to eliminate scanning and measuring biases.

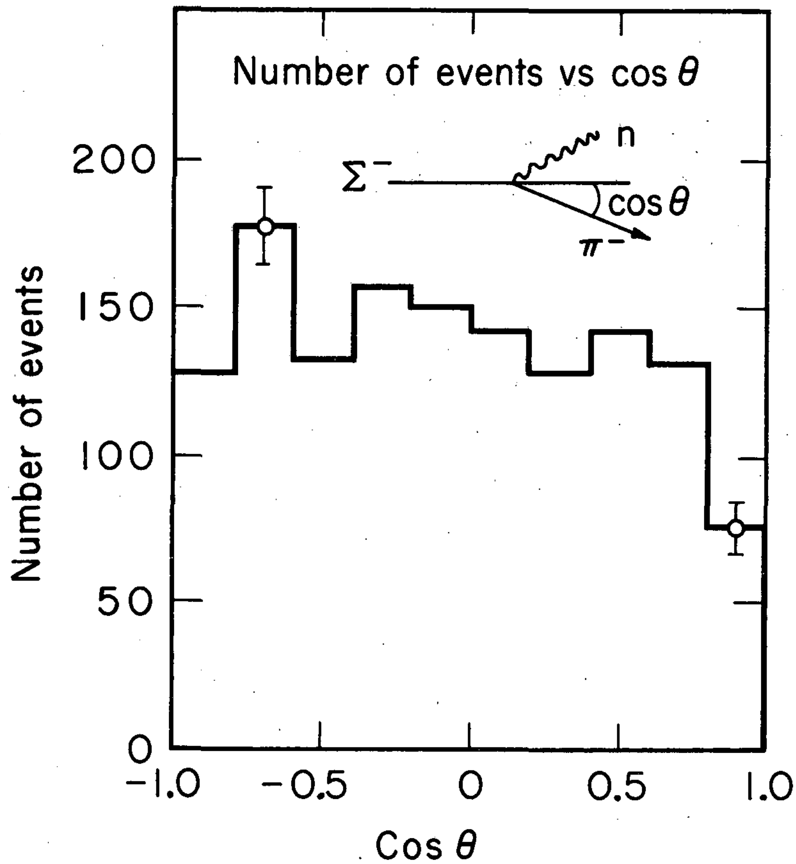

MU-34327

Fig. 2. Histogram of number of events vs the decay cosine in the rest frame; $\cos\theta_{\Sigma\pi} = 1$ corresponds to the π^- going forward.

We compute the sum of χ^2 and total constraints for the production and zero-or-more-decay fits. Events with either an overall confidence level of less than 0.1% or any individual fit less than 0.1% are rejected.[13] The corrections due to failing events are discussed in the following section.

We have two geometrical cutoffs: all decay and production origins must be within their respective fiducial volumes, and all unstable particles must be longer than a minimum length, L (5 mm for Λ and K^0, 3 mm for Σ^-). This amounts to an average escape correction of 2% for the fiducial volume and 10% for the minimum-length cutoff. We apply the correction on an event-by-event basis, according to the following considerations.

There are three possibilities for the fate of an unstable particle of momentum p, lifetime τ, and charged branching ratio b:[14]

(i) Charged decay less than L mm from the production vertex:

$$P_1 = b(1 - e^{-L/\eta c\tau}),$$

where η = p/Mass and c = velocity of light

(ii) Charged decay between L and the fiducial wall (good decays):

$$P_2 = b(e^{-L/\eta c\tau} - e^{-l/\eta c\tau}),$$

where l = distance to the wall.

(iii) Nonvisible decay; charged decay outside the volume, or neutral decay:

$$P_3 = be^{-l/\eta c\tau} + 1 - b.$$

The appropriate detection probability is then dependent on whatever configuration is taken to be the signature of the event. For Σ^-K^+ there is no confusion;[15] we count all events with a good Σ^-:

$$P_{\Sigma^-K^+} = P_2^{\Sigma}, \quad \text{with } b = 1.$$

For the Σ^0K^0 angular distribution we accept events with a good K^0 and no Λ of length less than L:

$$P_{\Sigma^0K^0} = P_2^K(1-P_1^{\Lambda}) \quad \text{with } b_K = 1/3,\ b_\Lambda = 2/3.$$

But for the Σ^0K^0 polarization we need a good K^0 and a good Λ, so

$$P_{\Sigma^0K^0}\,(\text{polarization}) = P_2^K P_2^{\Lambda}.$$

The ΛK factors are

$$P_{\Lambda K}\,(\text{angular distribution}) = P_2^{\Lambda}P_3^K + P_2^K P_3^{\Lambda} + P_2^K P_3^{\Lambda},$$

$$P_{\Lambda K}\,(\text{polarization}) = P_2^{\Lambda}(1-P_1^K).$$

The behavior of $P_{\Sigma^-K^+}$ and $P_{\Lambda K}$ (ang. dist.) as a function of center-of-mass angle is shown in Fig. 3.

Each event is weighted (i.e., corrected) by the inverse of its one or more detection probabilities, depending on how it's going to be used. The error, dY, in the sum of weighted counts, Y, is given by

$$Y \pm DY = \sum_{i=1}^{N} 1/\epsilon_i \pm \left[\sum_{i=1}^{N}\left(\frac{1}{\epsilon_i}\right)^2\right]^{1/2},$$

where N is the number of events and ϵ_i is the detection probability of the ith event.

C. Unpassed Events

Unpassed events are mainly the subset of χ^2 failures which are defined to be good after a suitable amount of re-examination or reprocessing, or both. These events do not appear in the histograms but are added as a correction (6%) to the final quoted cross sections.

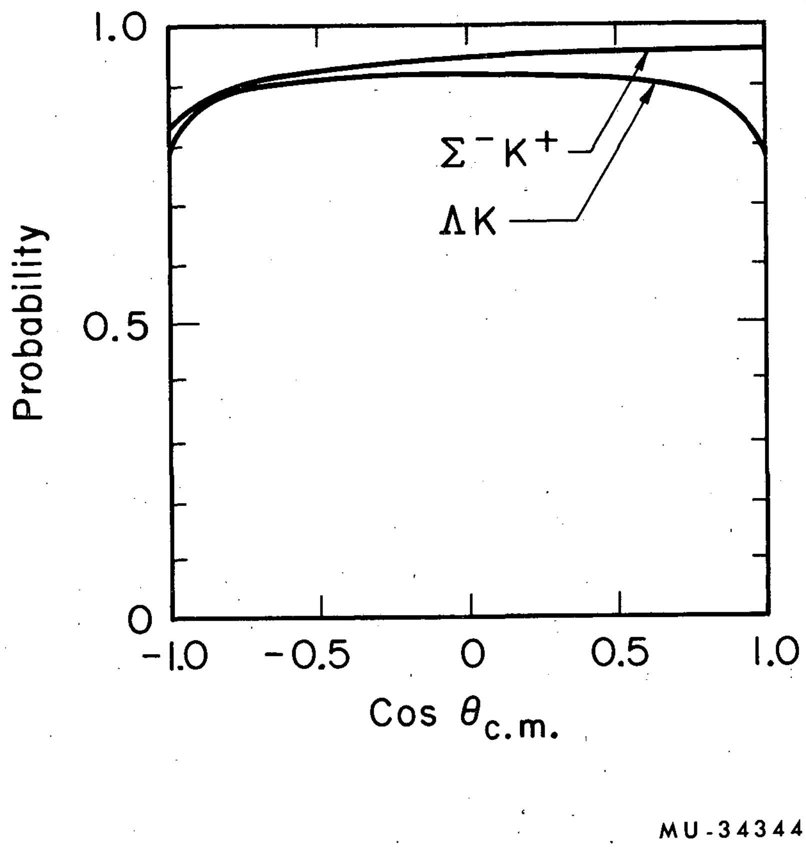

Fig. 3. Detection probability vs c.m. cosine for ΛK and $\Sigma^- K^+$. $\cos\theta = 1$ corresponds to the hyperon going forward. Only the effect of the minimum-length cutoff is shown. The finite chamber size has a much smaller effect ($\approx 2\%$) and is relatively independent of angle when averaged over all chamber positions.

Failures fall into three categories, with percent correction as follows: first-scan failures (3%), second-scan failures (1.5%), and events classified during the scanning as unmeasurable (1.5%).

All first-scan rejects were automatically remeasured, leaving 25% of the sample as failures. These events were re-examined on the scanning table and gross errors (wrong event types, nonevents) were corrected. After second remeasurement there remained 10% hard-core failures, which were subjected to the same rescan and measuring procedure, finally yielding 1.5% unpassed events. Unfortunately, some 500 additional rejects (3%) were overlooked owing to a bookkeeping error; 20% of these were re-examined and the final numbers of good events were estimated from this sample.

The second-scan events were measured twice and a sample of the remaining rejects was rescanned; 60% were estimated to be good, giving a correction of 1.5%.

The so-called unmeasurable events were all looked at and obvious nonevents discarded. The remaining events are assumed to be good (1.5%). There is a small additional number of genuinely difficult measurements which have failed owing to steeply dipping tracks or obscured vertices. These are included in this category.

D. Path-Length Determination

The standard bubble chamber path-length determination consists of a track count coupled with some method of estimating the beam contamination. In π^- film one usually scans for and measures large delta rays and bremsstrahlungs to determine the $e-\mu$ background. Rather than embarking on a new scanning effort, we use data from a previously existing rough beam scan along with the well-measured values of the total cross sections from Diddens et al.[16] to obtain a satisfactory normalization.

In the original beam scan the scanners were instructed to account for each track by counting the incoming tracks, outgoing tracks, and total interactions. Every fifth frame of 136 rolls, chosen more or less at random, was scanned. Frames with too many tracks were discarded. We must apply certain corrections to these data to get an unbiased estimate of the total number of interactions, N_T.

(i) The choice of rolls was actually somewhat spotty. A short supplementary scan of every twentieth frame in an additional 30 rolls was done to increase the accuracy in the estimate of N_T.[17]

(ii) The exclusion of frames with too many tracks (TMT) biases the estimate too low. A sample of 270 TMT's was scanned, yielding a mean of 28.3 tracks/TMT. The number of interactions at each beam momentum was prorated accordingly.

(iii) No fiducial volume restriction was imposed on the beam scan. The number of events outside the fiducial volume is estimated from the percentage of fitted events outside the fiducial volume (2.5%).

(iv) Frames which were skipped by the regular scanner were excluded from all tallies.

(v) The scanning inefficiency is estimated to be $2 \pm 2\%$, assuming that the missed events consist entirely of zero prongs and small-angle scatters.[18]

A count of the total number of frames is needed for conversion to μb/event. The final results are given in Table I.

E. Ambiguous Events

Events with two or more hypotheses satisfying the confidence-level tests (Section B) require a certain amount of extra attention. In the first approximation we can choose the hypothesis with the highest confidence level, and in fact it will be seen that this is adequate for most classes of ambiguities.

Table I. Summary, mb/event.

P_{beam}	Total cross section (mb)[a]	μb/event
1500	34.7	0.664
1690	34.3	0.457
1850	34.5	0.522
1950	35.4	0.441
2050	35.9	0.947
2150	35.7	0.354
2255	35.5	0.333
2360	34.5	0.683

[a] Interpolated from the values of Diddens et al. (reference 16).

1. Σ^- ambiguities

Two percent of the Σ^-K^+ events were ambiguous. Figure 4 is a scatter plot of the confidence levels of the two competing hypotheses, ΣK vs $\Sigma K\pi$. The 45° line corresponds to a division according to highest probability. The great majority of the events have high probability for ΣK and low probability for $\Sigma K\pi$, and as such are purely formal ambiguities. We conclude that less than 1% of the Σ^- events are true ambiguities.

2. Ambiguous V's

Fifteen percent of the single V's passed both Λ and K hypotheses. These were resolved (90%) by using the ionization of the positive prong of the V.

There were only two examples of double V's with (Λ, K) ambiguities.

3. Σ^0 - Λ separation--double-V events

Twenty-five percent of the ΛK's, pass as $\Sigma^0 K$. Of the $\Sigma^0 K$'s 20% pass as $\Lambda K\pi$. Figure 5 shows the relevant scatter plots. All the ($\Sigma^0 K^0$, $\Lambda K\pi$) events appear to be true ΣK; the highest-probability assignment results in a loss of five events to the three-body channel. The (ΛK, $\Sigma^0 K$) plot shows a substantial number of true ambiguities, and it becomes important to try to resolve them. A true ΛK event must be coplanar, but it is still possible for it to pass as $\Sigma^0 K^0$ if the γ lies in the plane of the reaction. The converse is not true: a true $\Sigma^0 K^0$ in general produces γ's lying out of the (π, Λ, K) plane, so that it will fail when tried as a ΛK essentially because of the lack of coplanarity. Thus true ΣK^0 will not fake ΛK, but true ΛK can fake $\Sigma^0 K$ so that all the ambiguous events are most likely ΛK and not $\Sigma^0 K^0$. Assignment on the basis of highest confidence level would result in biasing the $\Sigma^0 K^0$ channel 6% high.

4. Σ^0-Λ separation--single Λ events

Figure 6 is a histogram of the missing mass squared for events with a visible Λ. Since the Σ^0 events are unconstrained, there is no confidence-level test and the separation rests on the resolution of the

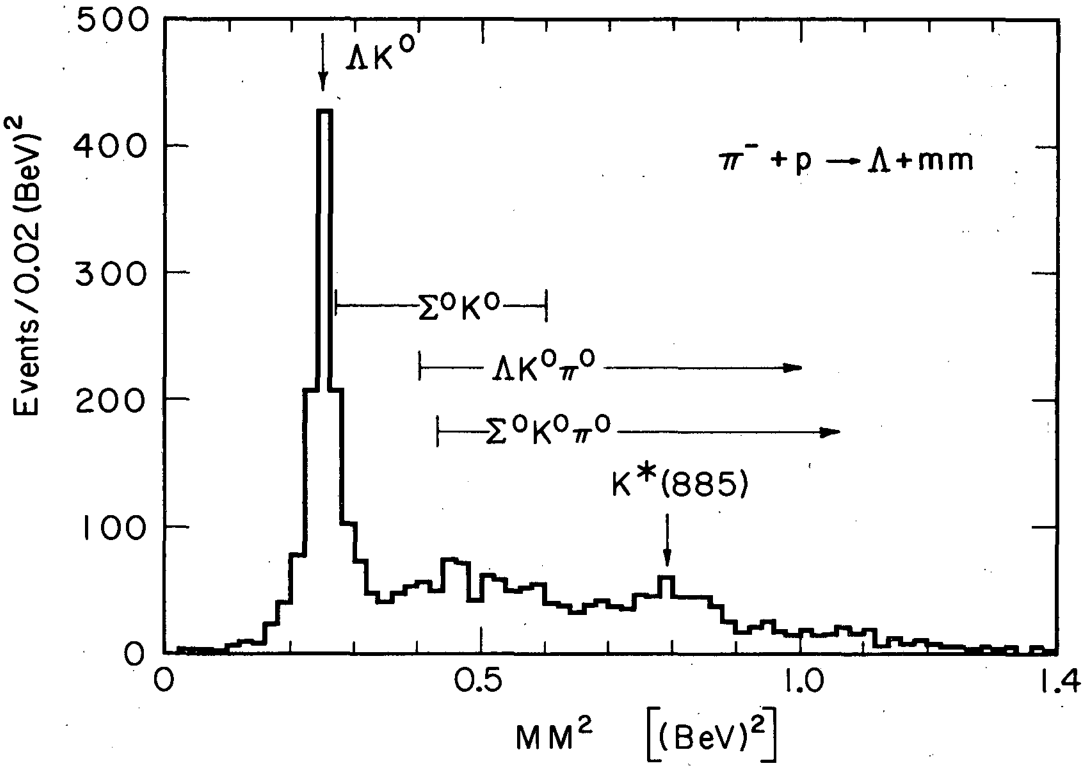

MU-34346

Fig. 6. Histogram of number of events vs the missing mass squared recoiling against the visible Λ for all single Λ events.

missing-mass spectrum. It turns out that the resolution is considerably worse for forward-produced Λ's than it is for backward ones. Figure 7 reveals a difference of about a factor of 2 in the resolution for the two cases. The unshaded region corresponds to events passing as ΛK. The backward events have about 2% background, estimated by extrapolation of the Σ^0 spectrum from 0.4 $(\mathrm{BeV})^2$ back to the kinematic limit. The forward events have a clearly asymmetric peak, and comparison with the low-mass side of the peak gives an estimated 15% background. We make a crude but adequate correction by imposing a cutoff of 0.32 $(\mathrm{BeV})^2$ on the missing mass.[19] This still leaves an estimated 3% contamination in the forward direction, but this is well within the statistics of any angular interval. The total contamination is less than 2%.

5. Σ^0-Λ separation–single K events

Figures 8 and 9 show the plots analogous to those of the preceding section for the single K events. The division based on highest confidence level is indicated by the cross-hatched areas in Fig. 9. There is negligible bias for the ΛK channel, since single K events enter into the final plots with a statistical weight of about 1/7. The cross section for ΛK production is twice that for Σ^0K, so that there is a net transfer of events from the ΛK to the Σ^0K channel in the overlap region for forward-produced K^0. A comparison of the low-mass side of the Λ peak and the high-mass side of the Σ^0 peak gives an estimated 15% contamination in the Σ^0K^0 channel. The statistical weight of single K events in Σ^0K^0 is about 1/3, so the bias is about 5%.

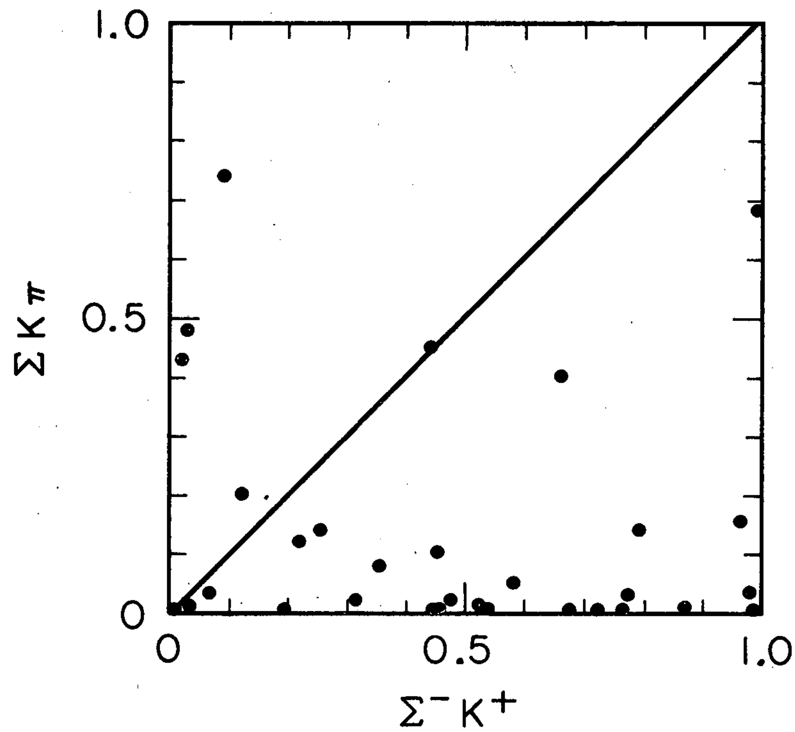

Fig. 4. Scatter plot of the confidence levels for the ambiguous Σ^-K^+ vs $\Sigma K\pi$. The 45° line corresponds to a division based on highest probability.

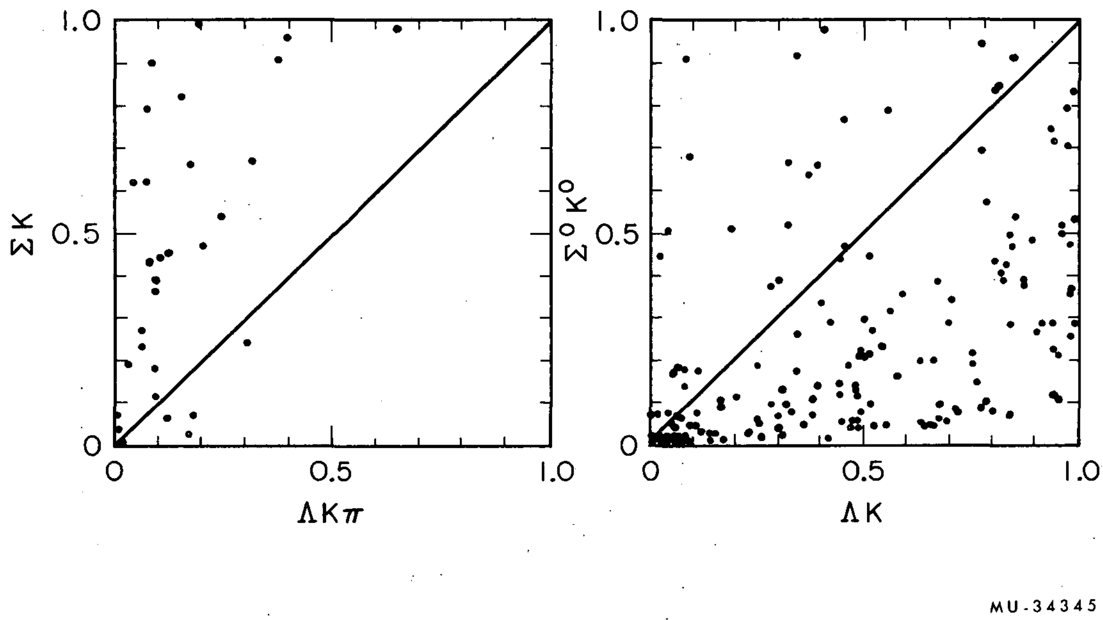

Fig. 5. Scatter plots of the confidence levels for ambiguous $\Sigma^0 K^0$ vs $\Lambda K\pi$ and ΛK vs $\Sigma^0 K^0$.

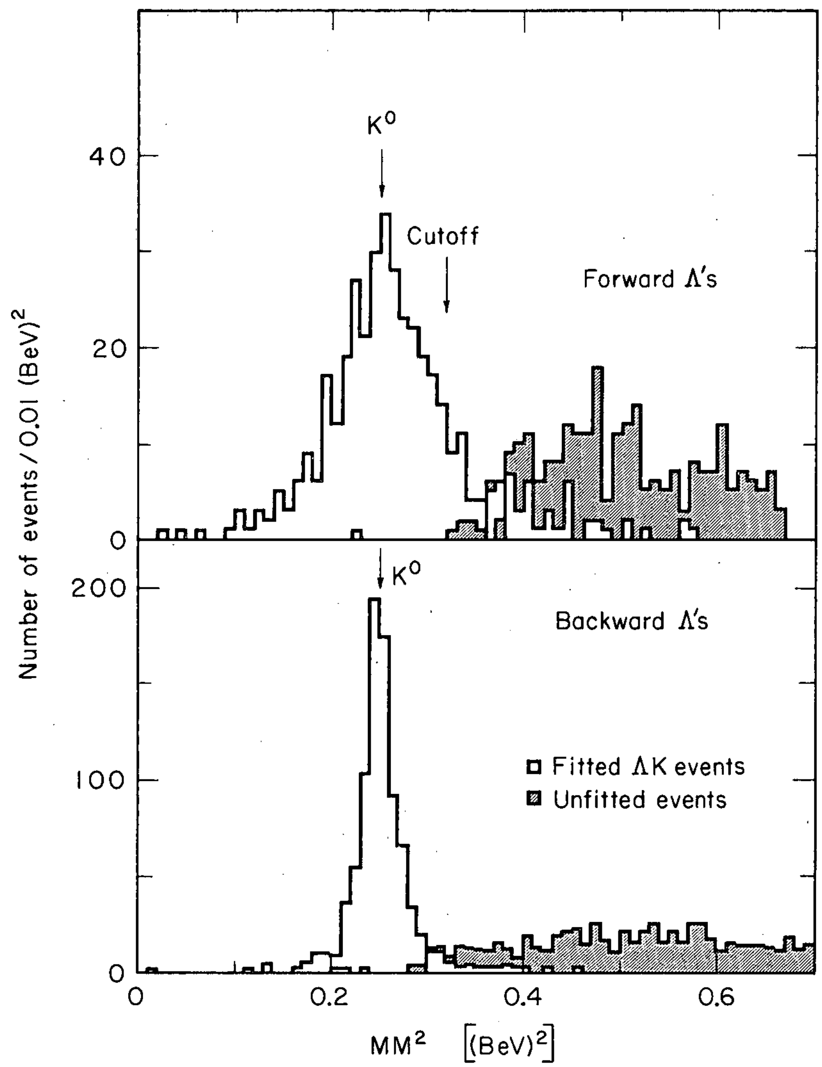

MU-34329

Fig. 7. Histograms of number of events vs the missing mass squared in single Λ events for the two angular intervals $-1 \leqslant \cos\theta \leqslant 0$ (bottom plot) and $0 \leqslant \cos\theta \leqslant 1$ (top plot). The unshaded region corresponds to events chosen as passing ΛK events. The kinematic limits of the Σ^0 spectra are for a beam momentum of 2000 MeV/c.

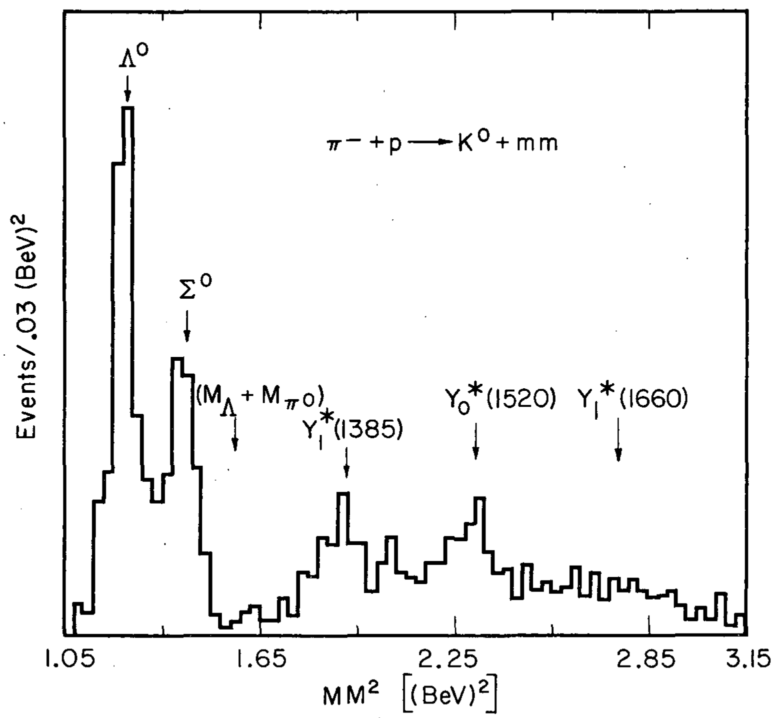

MU-34330

Fig. 8. Histogram of number of events vs the missing mass squared in single K events.

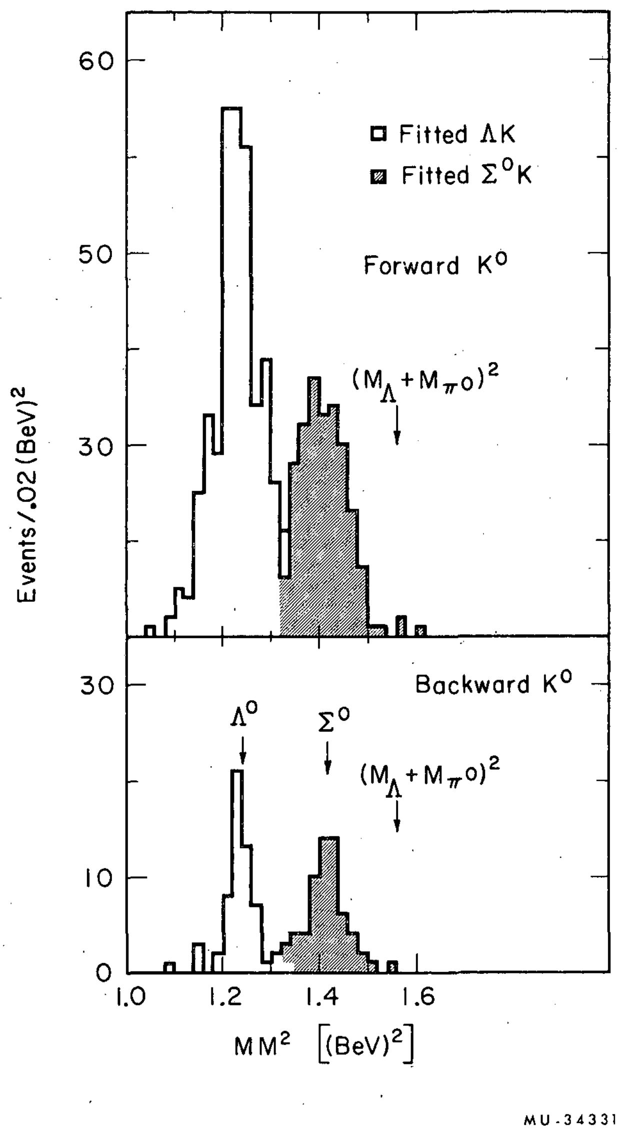

Fig. 9. Histograms of number of events vs the missing mass squared in single K events for the two angular intervals $-1 \leq \cos\theta \leq 0$ (bottom plot) and $0 \leq \cos\theta \leq 1$ (top plot). The hatched region is $\Sigma^0 K^0$; the unshaded region ΛK.

III. RESULTS

A. Cross Sections

The results for the three reactions are shown[20] in Fig. 10 and Table II. The rather large weights given in the table are actually quite well determined, since the big corrections are due to effects that can be estimated with great accuracy. For example, the minimum-length cutoff correction depends only on the lifetime of the particle. The overall normalization uncertainty is $\lesssim 3\%$, and comes from the inclusion of the unpassed events and the estimated efficiency of the beam scan. (Section IID.)

The cross sections fall off uniformly from 1.5 to 2.4 BeV/c with no evidence of any enhancement from the nucleon isobar $N^*_{1/2}(2190)$[21] at 2.05 BeV/c. The region in the vicinity of $N^*_{3/2}(1920)$ (P_π = 1.5 BeV/c) shows some evidence of a bump, but this may be spurious, since the effect appears to occur in all three channels ($N^*_{3/2}$ can't decay into the pure T = 1/2 ΛK state).

B. $\pi p \rightarrow \Sigma^0 K^0$

The angular distributions are shown in Fig. 11 fitted to a power series in $\cos\theta_{\pi\Sigma}$.[22] The distributions have a marked backward peak and a forward hump which seems to move backward with energy. The severity of the backward peak rules out a simple K^*-exchange model[23] of the form

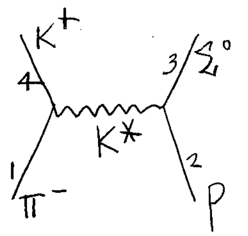

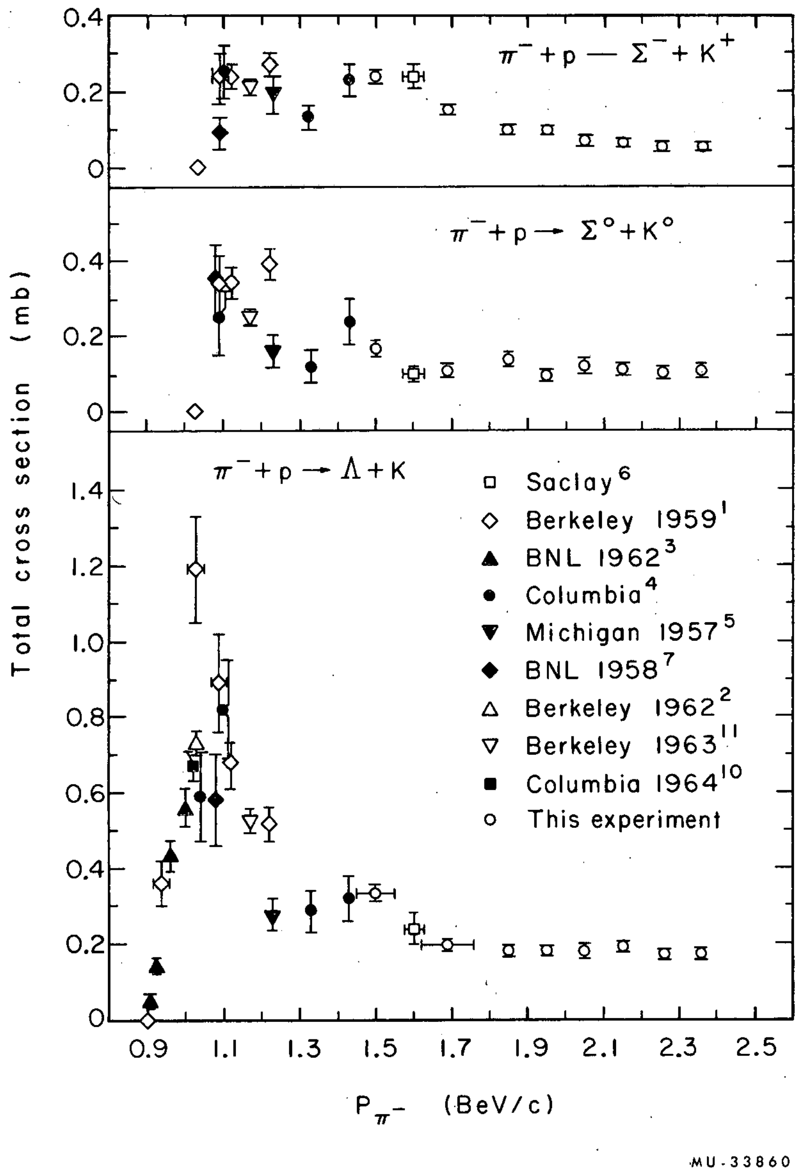

Fig. 10. Total cross sections for the reactions $\pi p \rightarrow YK$.

Table II. Total cross-section summary.

P_{beam}	$\pi^- + p \to \Lambda + K$			$\pi^- + p \to \Sigma^0 + K^0$			$\pi^- + P \to \Sigma^- + K^+$		
	Number of events	Weight[a]	σ (μb)	Number of events	Weight[b]	σ (μb)	Number of events	Weight	σ (μb)
1450-1550	308	1.27	334± 19	59	1.42	167± 22	293	1.25	242± 14
1620-1760	263	1.27	199± 12	58	1.36	110± 14	266	1.23	153± 9
1800-1900	215	1.25	181± 12	66	1.35	140± 17	153	1.24	99± 8
1900-2000	255	1.26	182± 11	53	1.34	94± 13	182	1.24	99± 7
2000-2100	119	1.26	182± 17	33	1.30	123± 21	60	1.22	70± 9
2100-2200	334	1.26	192± 11	82	1.31	114± 13	148	1.24	65± 5
2200-2310	319	1.26	172± 10	80	1.31	105± 12	138	1.25	57± 5
2310-2410	157	1.26	174± 14	41	1.34	113± 18	63	1.24	53± 7

[a] not including a factor 9/7 for the branching ratios.

[b] not including a factor 3/1 for the K^0 branching ratio.

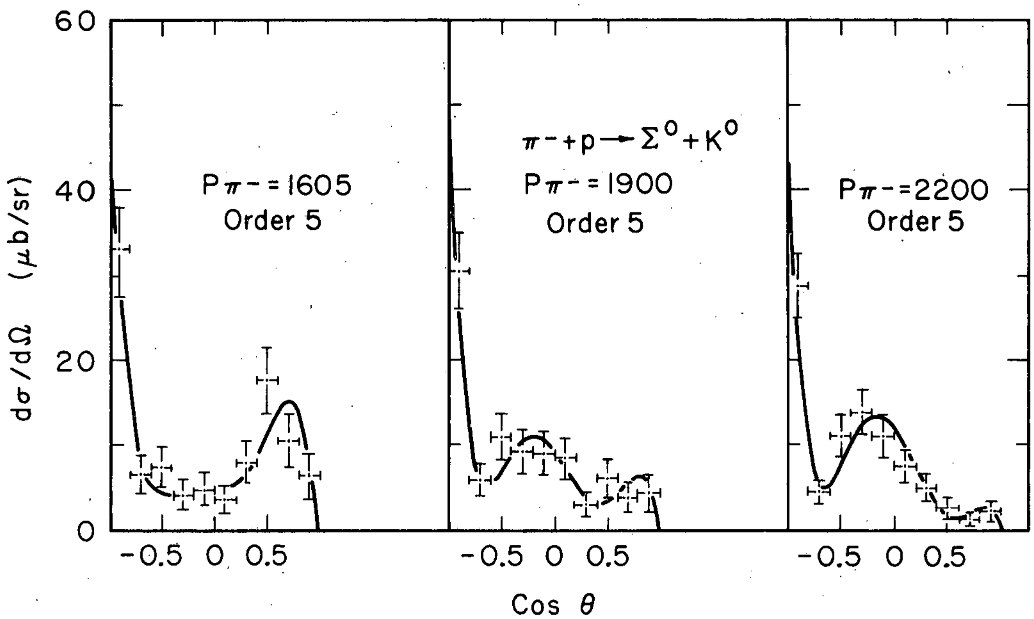

MU-34347

Fig. 11. Angular distributions for the reaction $\pi p \rightarrow \Sigma^0 K^0$. The smooth curves are least-squares fits to a power series in cos θ averaged over the histogram intervals. Cosθ = 1 corresponds to the Σ^0 going forward.

with matrix element

$$M = C\left(k_1+k_4\right)^{\mu}\left(-g_{\mu\nu}+\frac{q_{\mu}q_{\nu}}{M_{K^*}^2}\right)\overline{U}_{\Sigma^0}\,\gamma^{\nu}\,U_p\Big/\left(q^2-M_{K^*}^2\right),$$

where $q = k_2 - k_3$, $\overline{U}_{\Sigma^0}$, U_p are the Dirac spinors for the Σ^0 and proton, and the factor C contains the coupling constants and normalization factors for the boson and fermion wave functions. In addition, at $P_{\pi} = 2200$, the deep minimum at $\cos\theta = -0.7$ would tend to argue against the efficacy of adding background amplitudes, since it would take several partial waves to cause such an interference (Fig. 12).

The coefficients of the least-squares fit are given in Table III. There is a monotonic energy dependence for some of the terms, but no really firm conclusions can be drawn because of the limited statistics.

C. $\pi p \to \Sigma^- K^+$

Since there are no known $T = 3/2$ mesons, one-meson exchange is ruled out for this channel, and in fact the distributions in $\cos\theta_{\pi\Sigma}$ are all forward-peaked (Fig. 13), confirming our expectations and suggesting the presence of a baryon-exchange mechanism

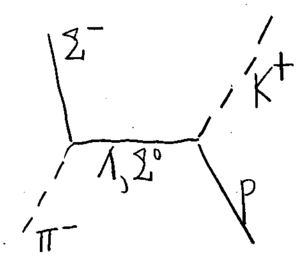

which could produce backward K^+ and forward Σ^-.

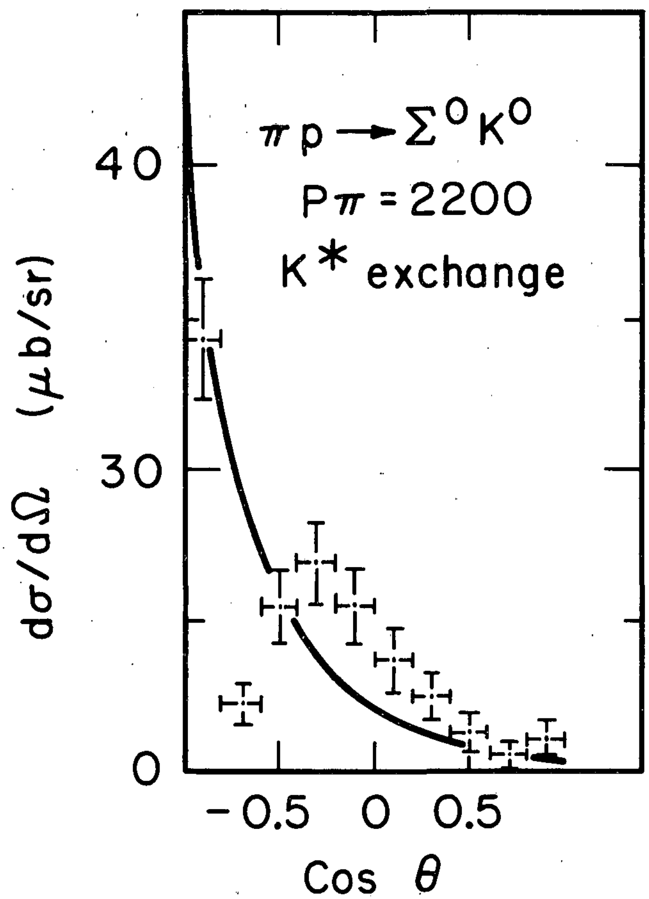

MU-34332

Fig. 12. Angular distribution for $\pi p \rightarrow \Sigma^0 K^0$ at $P\pi = 2200$ MeV/c, showing the prediction of the K^*-exchange model. The curve is normalized to the total area.

Table III. Coefficient of the least-squares fits for $\pi p \rightarrow \Sigma^0 K^0$.

An(μb/sr)	P beam (MeV/c) 1606	1900	2200
A_0	4.4± 1.2	9.2± 1.5	11.8± 1.3
A_1	0.7±6.3	-17±6.3	-18± 5
A_2	12± 11	-28± 10	-46± 8
A_3	49± 29	73± 25	70± 20
A_4	6± 15	44± 13	58± 10
A_5	-77± 29	-83± 25	-77± 19

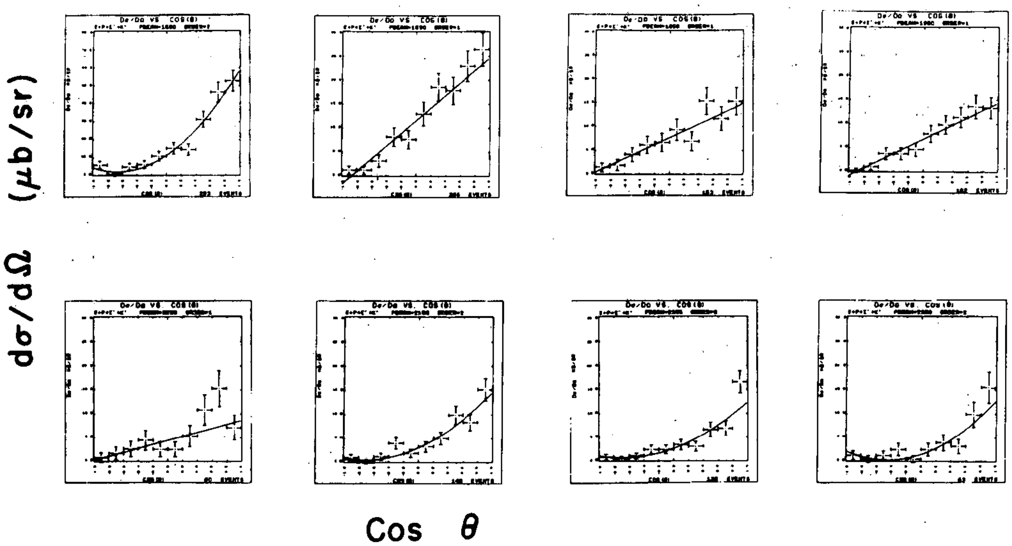

MU-34382

Fig. 13. Angular distributions for the reaction $\pi p \to \Sigma^- K^+$. The smooth curves are least-squares fits to a power series in $\cos\theta$ averaged over the histogram intervals.

The plot of the coefficients of the least-squares fit against energy (Fig. 14) shows no significant structure except that there appears to be a large A_1 coming in at $N^*_{3/2}(1920)$ and then going out again. This is probably a coincidence having to do with the relative phases of the s- and p-wave amplitudes rather than a manifestation of a resonant state, since there is no evidence for any higher powers of $\cos\theta$ in the distribution. Similarly the plot at $P_\pi = 2050$ is suggestive of a contribution from some high partial wave, and the fit can be somewhat improved 60% vs 10% probability by going up through $\cos^5\theta$. If this behavior persisted at $P_\pi = 2150$ or 1950 we could interpret it as the decay of $N^*_{1/2}(2190)$ into $\Sigma^- K^+$, but neither of these plots has any evidence of high powers in it.

One other feature of the data is worth mentioning. The absence of $\cos^2\theta$ from 1690 to 2150 Mev/c might ordinarily be interpreted as the absence of the $P_{3/2}$ amplitude. The Yang ambiguity, however, predicts that the angular distribution is invariant under the transformation[24]

$$S^T_{1/2} = S^*_{1/2},$$

$$P^T_{1/2} = 4\,P^*_{3/2} - (1/3)\,P^*_{1/2},$$

$$P^T_{3/2} = (P^*_{3/2} + 2\,P^*_{1/2})/3,$$

so that a distribution with $P_{3/2}$ nominally equal to zero is identical to one in which $P_{3/2} = -2P_{1/2}$. The presence or absence of this kind of accident is determined by examining the system at energies below the one(s) in question. If there is a consistent lack of $\cos^2\theta$ then one usually assumes that this relation does not persist down to the threshold, where the amplitude in question is likely to become important. In our case the existence of a large $\cos^2\theta$ term at 1500 MeV/c and its reappearance at 2150 MeV/c suggest that $P_{3/2}$ has not become small but that the above relationship between $P_{3/2}$ and $P_{1/2}$ holds. A

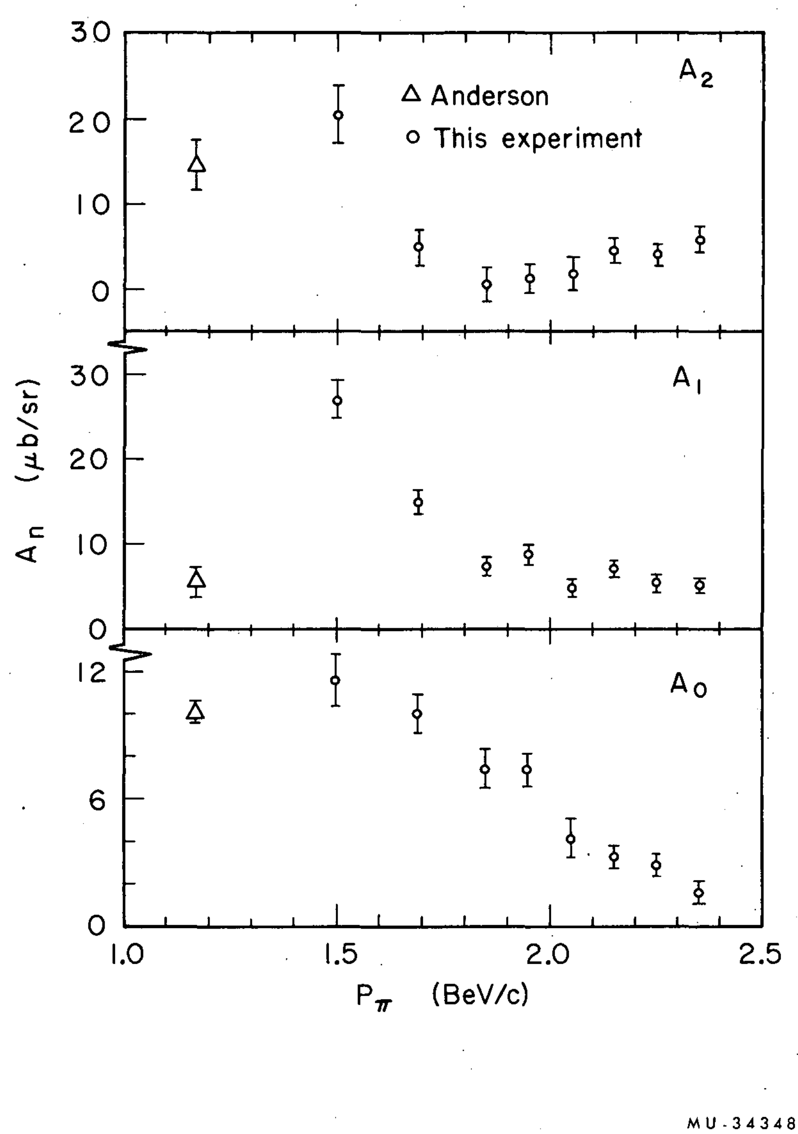

Fig. 14. Coefficients of the least-squares fit vs beam momentum for the reaction $\pi p \rightarrow \Sigma^- K^+$.

limited search for the amplitudes using the 7090 program MINFUN shows that the most natural (in the sense of least violent) energy dependence of the amplitudes favors a true decrease of $P_{3/2}$ term over the Yang-transformed solution.[25] I have no explanation of why this should occur, however.

D. $\pi p \to \Lambda K$

The gross features of the data are the severe backward peak and the large polarization in the backward direction (Figs. 15 and 16). The polarization, $P(\theta)$, for a given angular interval is calculated by

$$\alpha_{\Lambda} P(\theta) \frac{d\sigma}{d\Omega} = 3\left[\sum_i \xi_i/\epsilon_i \pm \left\{\sum (\xi_i/\epsilon_i)^2\right\}^{1/2}\right],$$

where ξ is the cosine of the angle of the decay π^- with respect to the normal to the production plane, $\vec{P}_\Lambda \times \vec{P}_{beam}$, ϵ_i is the detection probability. The forward peak at $P_\pi = 1500$ decreases rather uniformly with increasing energy.

1. Analysis of $N^*_{1/2}(2190)$

Figures 17-20 show the coefficients of the least-squares fit to the angular distribution. The systematic fluctuations of the odd coefficients, in the vicinity of the resonance can be interpreted as evidence for the production and decay chain $\pi p \to N^*_{1/2}(2190) \to \Lambda K$. Since the effect is marginal I will simply sketch the lines a detailed analysis might take.

Table IV gives the expansions of the coefficients in terms of the partial waves.[26] The rising A_6 term (Fig. 20) indicates a background amplitude of $F_{7/2}$ or $G_{7/2}$. Since $l = 3$ is more likely to appear before $l = 4$, let us assume that the highest background wave is $F_{7/2}$. Then to the extent that the data exclude a significant A_8 term,[27] the resonance is limited to $G_{7/2}$ or $G_{9/2}$. Now write the resonant amplitude, T, as a Breit-Wigner form,

$$T = \frac{\sqrt{\frac{\Gamma_{\pi p}\,\Gamma_{\Lambda K}}{4}}}{E_0 - E - i\Gamma/4}$$

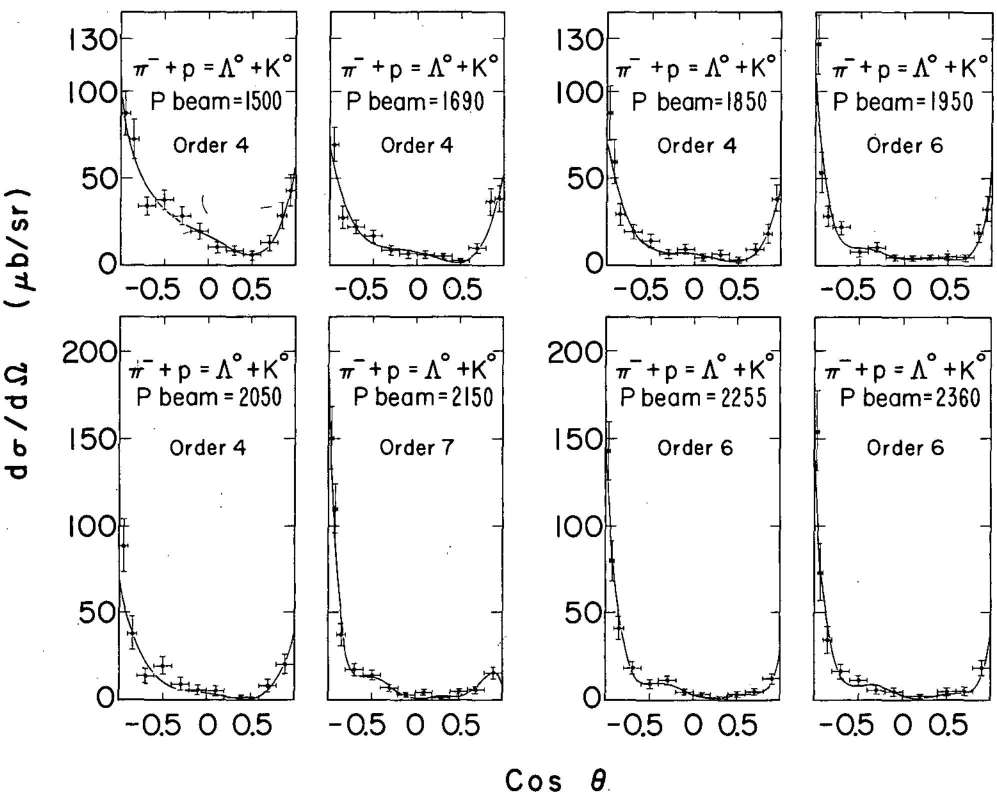

Fig. 15. Angular distributions for the reaction $\pi p \rightarrow \Lambda K$. The smooth curves are a least-squares fit to Legendre polynomials averaged over the histogram intervals.

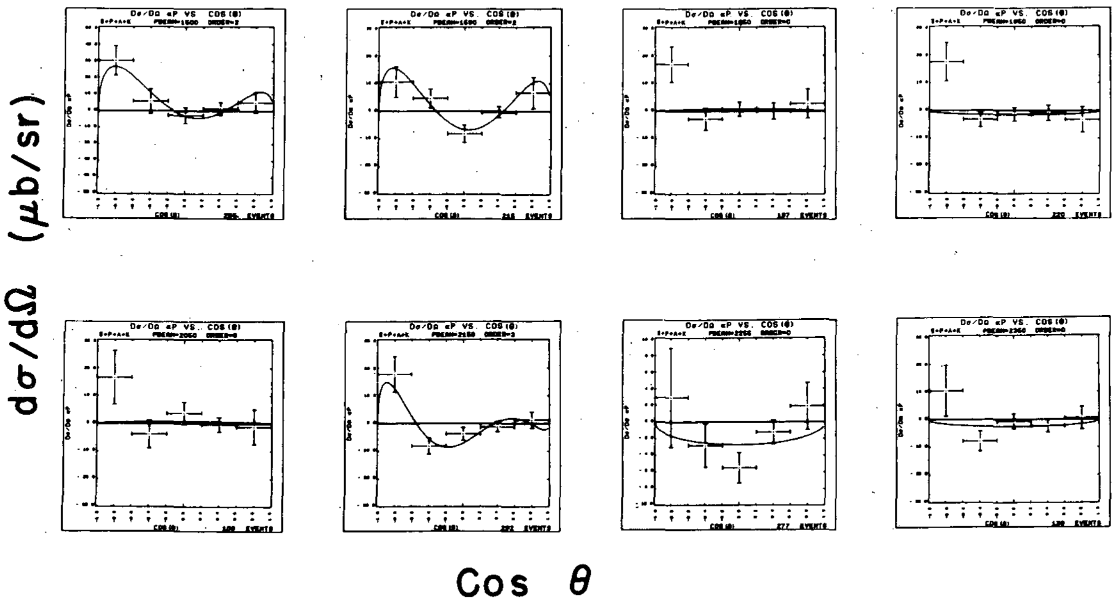

MU-34383

Fig. 16. Distributions of polarization, $\alpha_\Lambda P(\theta)\, d\sigma/d\Omega$, for the reaction $\pi p \rightarrow \Lambda K$. The normal to the production plane is taken to be $\vec{P}_\Lambda \times \vec{P}_\pi$. The smooth curves are of form $\sin\theta\, \Sigma\, b_n \cos^n\theta$ averaged over the histogram intervals.

0 0 0 0 2 3 0 2 4 8 2

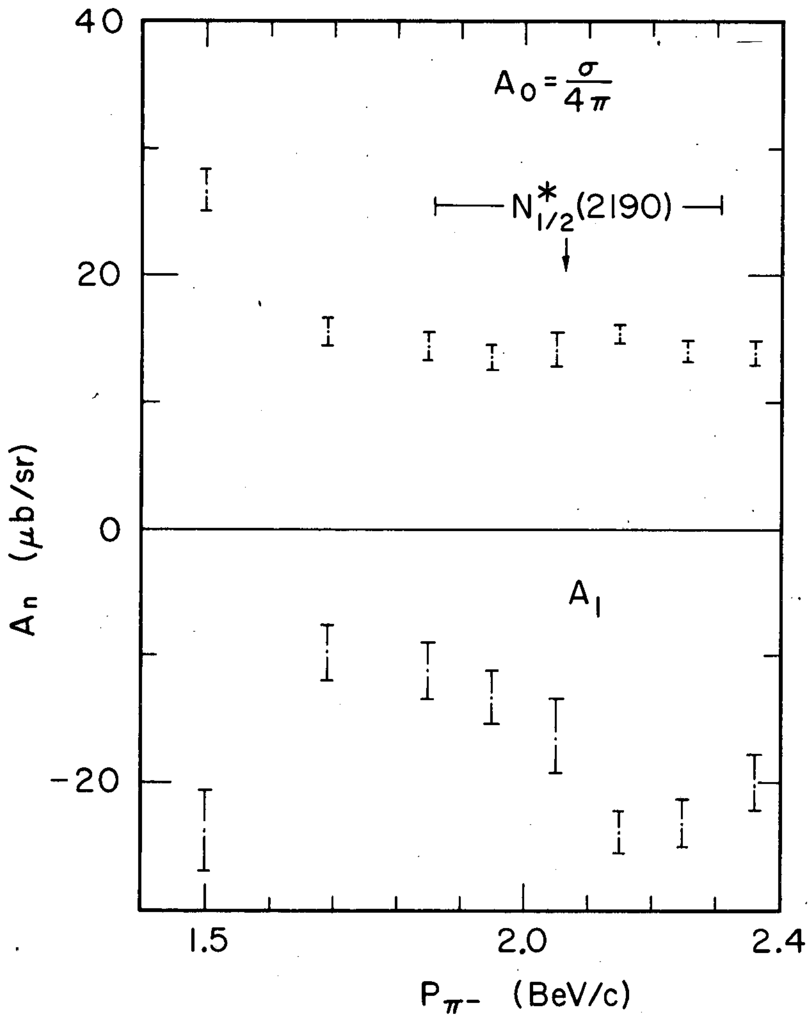

MU-34349

Fig. 17. Coefficients of the least-squares fit for the reaction $\pi p \rightarrow \Lambda K$ vs beam momentum, A_0 and A_1.

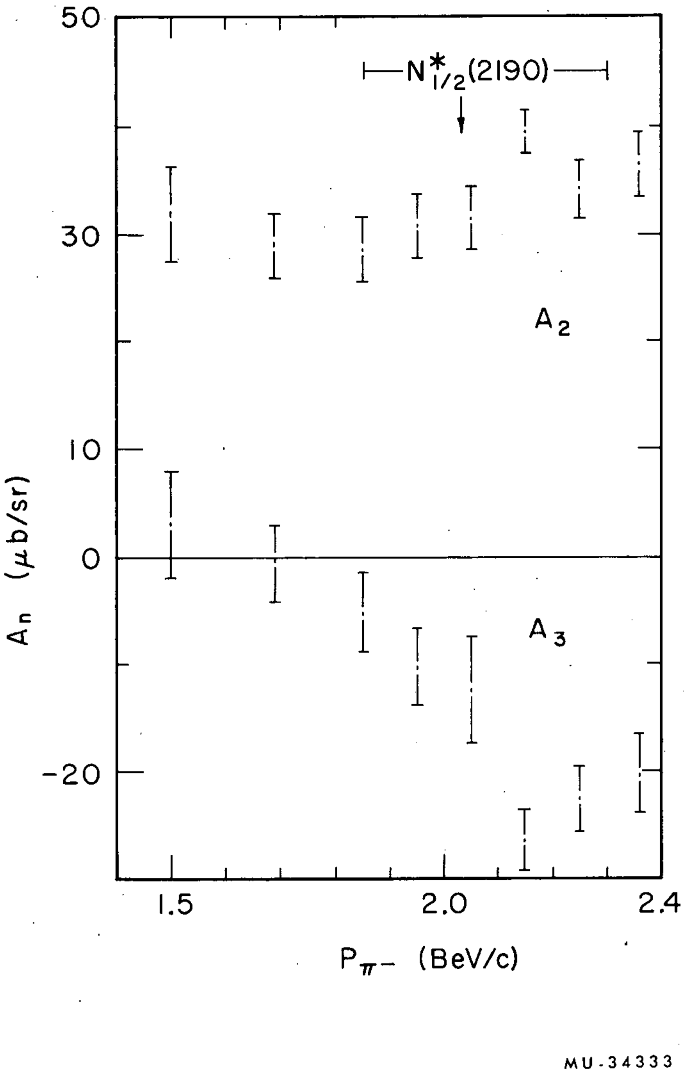

Fig. 18. Coefficients of the least-squares fit for the reaction $\pi p \rightarrow \Lambda K$ vs beam momentum, A_2 and A_3.

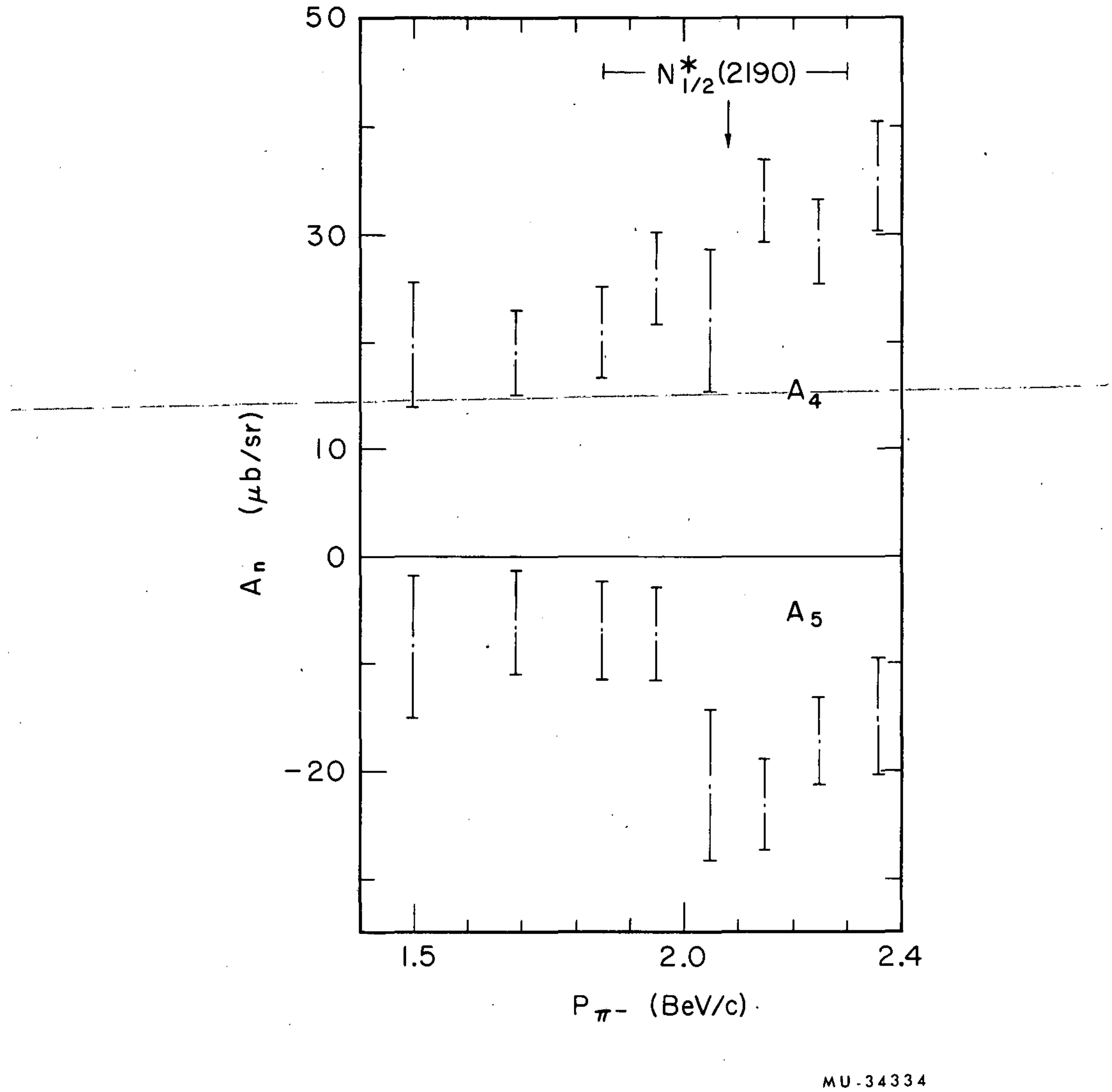

Fig. 19. Coefficients of the least-squares fit for the reaction $\pi p \rightarrow \Lambda K$ vs beam momentum, A_4 and A_5.

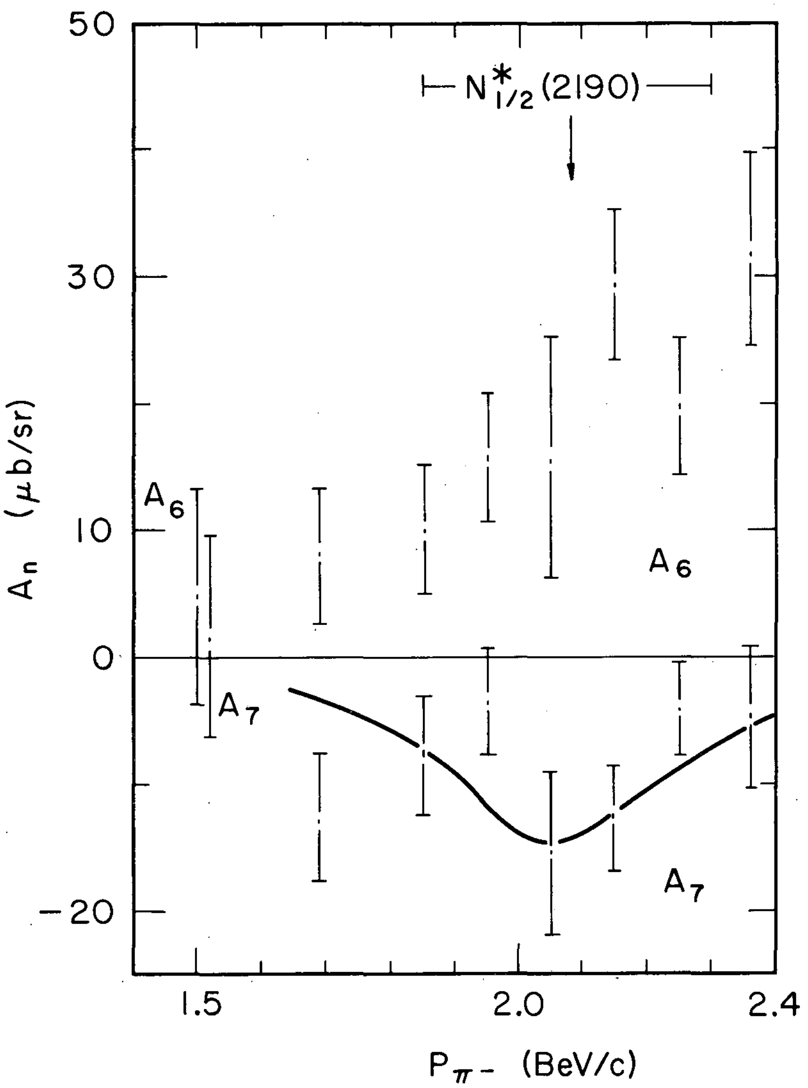

MU-34335

Fig. 20. Coefficients of the least-squares fit for the reaction $\pi p \rightarrow \Lambda K$ vs beam momentum, A_6 and A_7.

Table IV. Expansion of the coefficients $\sum_{n=0}^{8} A_n P_n(\cos\theta)$ in terms of the partial waves

	A_0	A_1	A_2	A_3	A_4	A_5	A_6	A_7	A_8
S1S1+P1P1	1								
S1P1		2							
S1P3+P1D3[a]		4							
S1D3+P1P3			4						
S1D5+P1F5			6						
S1F5+P1D5				6					
S1F7+P1G7				8					
S1G7+P1F7					8				
S1G9+P1H9					10				
S1H9+P1G9						10			
P3P3+D3D3	2		2						
P3D3		4/5		36/5					
P3D5+D3F5		36/5		24/5					
P3F5+D3D5			12/7		72/7				
P3F7+D3G7			72/7		40/7				
P3G7+D3F7				8/3		40/3			
P3G9+D3H9				40/3		20/3			
P3H9+D3G9					40/11		180/11		
D5D5+FsF5	3		24/7		18/7				
D5F5		18/35		16/5		100/7			
D5F7+F5G7		72/7		8		40/7			
D5G7+F5F7			8/7		360/77		200/11		
D5G9+F5H9			100/7		720/77		70/11		
D5H9+F5G9				20/11		80/13		3150/143	
F7F7+G7G7	4		100/21		324/77		100/33		
F7G7		8/21		24/11		600/91		9800/429	
F7G9+G7H9		40/3		120/11		120/13		2800/429	
F7H9+G7G9			200/231		3240/1001		280/33		3920/143
G9G9+H9H9	5		200/33		810/143		160/33		490/143

[a] Read expressions such as this as $\mathrm{Re}(S^*_{1/2} P_{3/2} + P^*_{1/2} D_{3/2})$, etc.

where $E_0 = 2190$, $\Gamma = 200$,[16] and $\Gamma_{\pi p}$, $\Gamma_{\Lambda K}$ are the partial widths for the πp, ΛK channels. This is re-expressed, by dividing through by $\Gamma/2$, as

$$T = \frac{x}{\epsilon - i} ,$$

which is a circle in the complex T plane with radius $x/2$ and centered at $(0, x/2)$. The background, B, is written as $B = re^{i\phi}$ and assumed to be energy-independent. Thus

$$\mathrm{Re}\, T^* B = \frac{rx}{\epsilon^2 + 1} [\epsilon \cos\phi + \sin\phi]$$

represents the behavior of the A_7 term. The curve in Fig. 20 corresponds to the choice $\phi = -90^0$, $x = 15\,\mu b/sr$. The fit is fair, but is expected to serve only as a rough guide to the possible behavior of the resonant terms. Refinements to the above expression would take into account the obvious energy dependence of the background and the angular momentum barrier[28] $(kr)^{l+1}$, which would produce a skewness to the resonance shape by suppressing the low-energy side and enhancing the high-energy side. A definitive analysis with improved statistics would include the polarization information and the rest of the coefficients, A_0 through A_5, and possibly higher-order terms.

The Regge pole theory[29] predicts an $N^*_{1/2}$ at 2190 MeV with spin-parity $H_{9/2}$ as the second recurrence of the nucleon. Kycia and Riley[30] have pointed out that the nucleon resonances seem to obey the empirical rule

$$J - L = I - 1.$$

Thus the $I = 1/2$ resonances follow the sequence $P_{1/2}(940)$, $D_{3/2}$ (1512), $F_{5/2}(1688)$, implying that $N^*(2190)$ is $G_{7/2}$. The $G_{7/2}$ assignment is somewhat favored by the present data.

2. K^* Exchange and Regge Poles

Simple K^* exchange with the matrix element of Section III D gives the results shown in Fig. 21. A least-squares fit to $\log(d\sigma/d\Omega)$

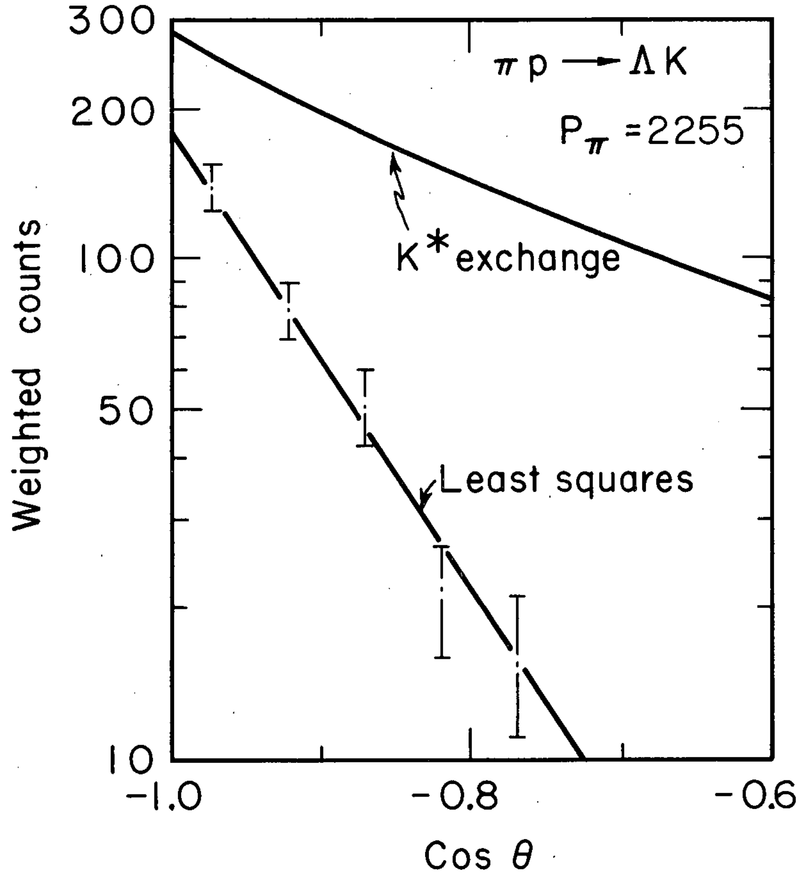

MU-34350

Fig. 21. Angular distribution for low momentum transfers in the reaction $\pi p \rightarrow \Lambda K$. The K^*-exchange curve is not normalized.

is given for comparison. The exchange model has about half the slope required by the data. Introducing form factors in place of the bare coupling constants would improve the fit but couldn't account for the large observed polarization. Thus we need to add background amplitudes in addition to the exchange term. Rather than continue in this vein of peripheralism and its variations, we can appeal to the recent Regge-pole analyses of backward (diffraction) scattering as suggested by Wagner and Sharp.[31] They give the asymptotic expression

$$d\sigma/d\Omega\,(S \to \infty) = f(t)(S/S_0)^{2\alpha(t)-1}\,.$$

where $S^{1/2}$ is the total c.m. energy, $t^{1/2}$ is the momentum transfer, and S_0 is an arbitrary constant; $\alpha(t)$ is the K^* trajectory, which for low momentum transfers we write as

$$\alpha(t) \approx \alpha(0) + \alpha'(0)\,t,$$

and then
$$d\sigma/d\Omega\,(S \to \infty) = g(s,t)\,e^{At}$$

with
$$A = 2\alpha'(0)\,\ln(S/S_0)$$

is the celebrated logarithmic shrinking of the backward (diffraction) scattering peak.

The procedures for arriving at this result are actually quite straightforward, but their justification is subject to question and is discussed in some detail in Squires' book.[32] I will outline the way in which these expressions develop. Complete presentations have been given by Frautschi,[33] Omnes and Froissart,[34] and Squires.[32] The papers of Kummer[35] and Jones and Poirier[36] are a useful introduction to these books. The experimental situation has been reviewed by Lindenbaum.[37]

Take elastic scattering of equal-mass spinless particles for the usual reasons,

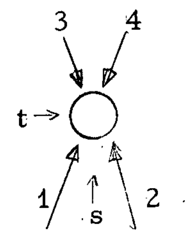

For the reaction in the t channel, $1+3 \rightarrow \overline{2}+\overline{4}$, the invariant amplitude is written

$$A(s,t) = \sum (2l+1)\, a_l(t)\, P_l(\cos\theta_t).$$

Regge used the Sommerfeld-Watson transform to write this as a contour integral in the complex l plane,

$$A(s,t) = -\frac{1}{2i} \int_C dl \, \frac{(2l+1)\, a(l,t)\, P_l(-\cos\theta_t)}{\sin\pi l},$$

with the contour of Fig. 22a. Our aim is to invoke crossing symmetry and go to the high-s, low-t limit and thus relate low-energy t-channel behavior to high-energy s-channel behavior.

With

$$\cos\theta_t = 1 + \frac{s}{2qt^2}, \quad q_t^2 = \frac{t}{4} - M^2$$

and
$$\underset{Z\to\infty}{P_l(z) \rightarrow} Z^{l_R + il_I},$$

the present contour gives a divergent behavior for $S \rightarrow \infty$. This is corrected by shifting the contour as in Fig. 22b, with the result

$$A(s,t) = -\frac{1}{2i} \int_{C_1} dl \, \frac{(2l+1)\, a(l,t)\, P_l(-\cos\theta_t)}{\sin\pi l}$$

$$- \sum_{i=1}^{N} (2a_i(t) - 1)\beta_i(t)\, P_{a_i}(-\cos\theta_t)/\sin\pi a_i,$$

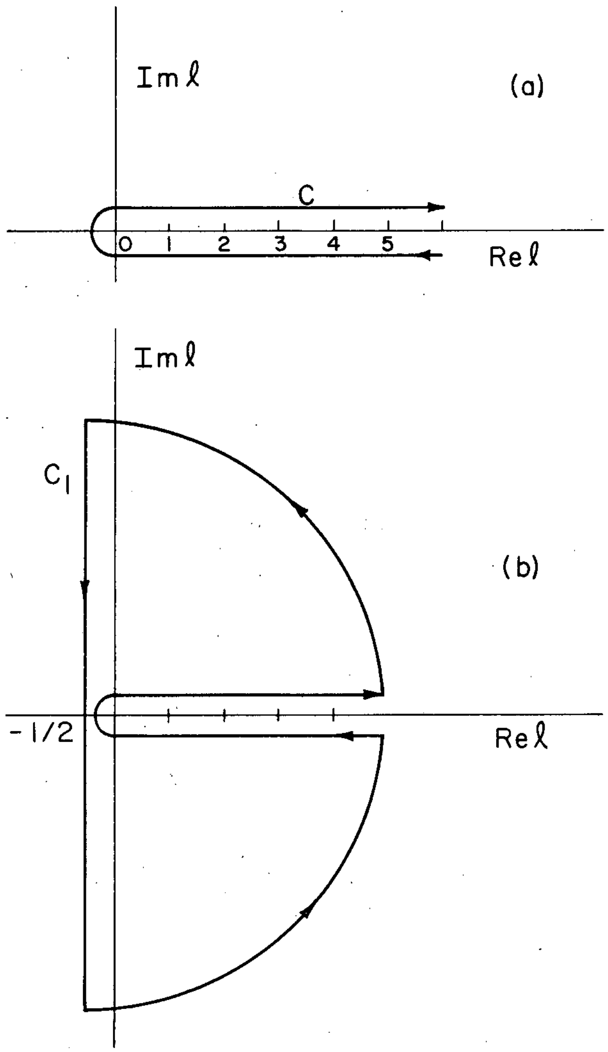

Fig. 22. (a) Contour for the Sommerfeld-Watson transform. (b) Shifted contour to insure convergent high-s behavior.

where the sum is over the poles encountered in opening up the contour, and the integral over the semicircle has been shown to vanish. (We ignore the existence of cuts.) Now take $S \to \infty$. The integral is small (owing to the factor $Z^{-1/2}$) compared with the summation, and we get

$$A(s,t) = -\sum_{L=1}^{N} \frac{(2\alpha_i+1)\beta_i(5/2q_t^2)^{\alpha_i(t)}}{\sin \pi\alpha_i}.$$

For scattering in the s channel, $t < 0$ and $\operatorname{Im}\alpha_i(t)$ has been shown to vanish. Further, the sum is dominated by the highest-lying pole, the so-called one-pole model, and the cross section is then

$$d\sigma/d\Omega = \frac{1}{s}\left|A(s,t)\right|^2 = g(t)\, S^{2\alpha(t)-1}.$$

This can be compared with peripheralism in the diagram

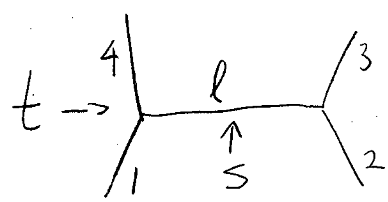

with the exchange of a particle with spin l. The amplitude in the t channel must be of the form[38]

$$A(s,t) \sim \frac{P_l(\cos\theta_t)}{t-\mu^2}\, g_1(t)\, g_2(t),$$

since the scattering goes entirely through the $\underline{l}$th partial wave. Thus for $s \to \infty$

$$A(s,t) \to \frac{s^l}{t-\mu^2}\, g_1(t)\, g_2(t),$$

as opposed to the Regge pole case, in which $l = l(t)$.

The black-disk model is also frequently invoked in elastic scattering.[39] In the scattering amplitude

$$f(\theta) = \frac{1}{2ik} \sum (2l+1)[\eta_l \exp(2i\delta_l) - 1] P_l(\cos\theta)$$

assume that there is complete absorption up through $l = L_{max} (\eta_l = 0)$. Then the sum is replaced by an integral over the impact parameter, b (where $kb = l + 1/2$), and the cross section is then given by

$$d\sigma/d\Omega = R^2 \left[\frac{J_1(kr\sin\theta)}{\sin\theta}\right]^2 \qquad kR = L_{max}$$

Following Lindenbaum,[37] we can rewrite this as

$$d\sigma/dt = \frac{\pi R^2}{4} \exp[-(R/2)^2 t]$$

for $t \leqslant 0.3$ $R \approx 1$ fermi, which is a nonshrinking exponential behavior.

We now consider the application of these results to $\pi p \rightarrow \Lambda K$. Two further points:

(a) the problem of which Regge pole dominates the reaction doesn't arise, since K^* exchange is the only allowed particle;

(b) we must have $\cos\theta_t \gg 1$ so that the asymptotic expansions are valid.

We are in a marginal range, since[40]

$$3 \leqslant \cos\theta_t(s) \leqslant 10,$$

thus the validity of the model is somewhat questionable. Nonetheless we forge blindly ahead.

The angular distributions are fitted to a form

$$\ln d\sigma/d\Omega = a + b\cos\theta$$

and with $$d\sigma/d\Omega = g(t)\, e^{At}$$

we have $$A = -b/2pp_0 ,$$

where p and p_0 are the average c.m. momenta of the proton and Λ.

The values of A for momentum transfer cutoffs of -0.4 and -0.3 are shown in Figs. 23 and 24. The fits are of the form[41]

$$A = c + d \ln(s - 1.4),$$

where $d = 2\alpha'(0)$ is the measure of the shrinking. The results obtained in this way are[42]

$$\alpha'(0)\ (t_c = -0.4) = 2.2 \pm 0.8\ (\mathrm{BeV}/c)^{-1},$$
$$\alpha'(0)\ (t_c = -0.3) = 1.4 \pm 1.1\ (\mathrm{BeV}/c)^{-1}.$$

The discrepancy between the two is because at the lower beam momentum points, 1500 and 1690 MeV/c, the slopes are a sensitive function of the cutoff; the smaller the cutoff the steeper the slope. This is reasonable, since background is expected to be more prominent here. Figure 25 shows the values of $2\alpha'(0)$ obtained as a function of the cutoff. The strong dependence on t_c is bad, but the results still indicate that shrinking does occur, although any estimate of the slope is obviously unreliable. It would be desirable to extend this study into the higher energy regions to see if the effect persists.

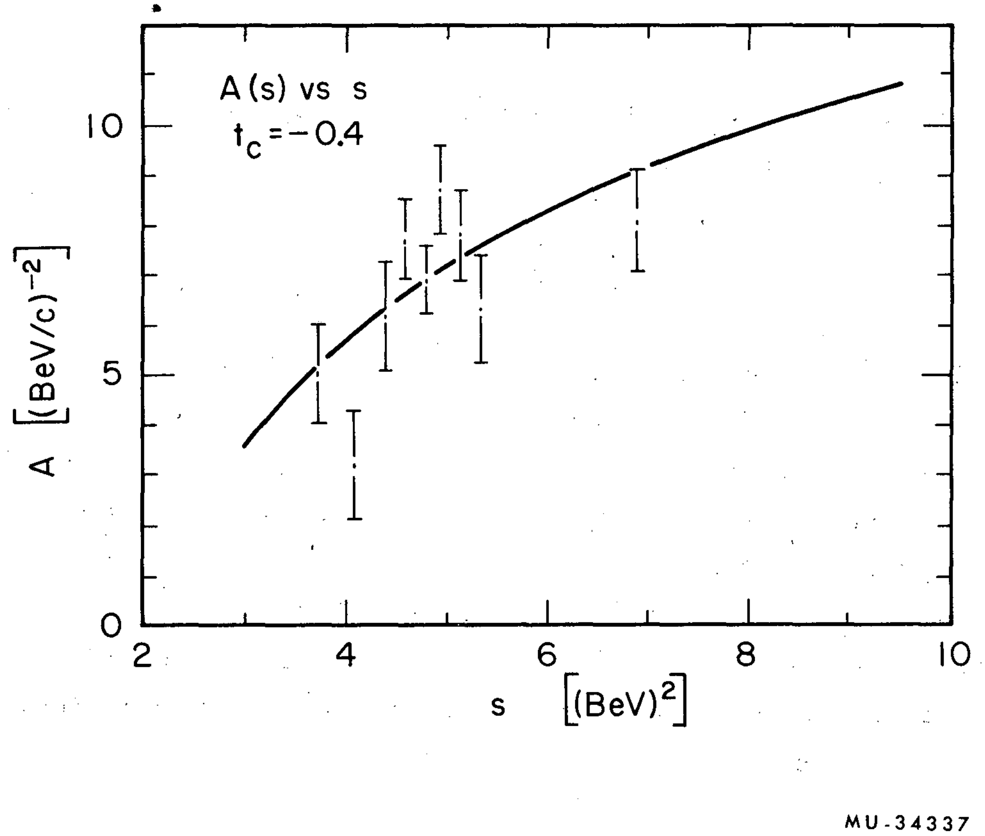

Fig. 23. Values of A(s) from the fits to $d\sigma/d\Omega = \sigma_0 e^{At}$ vs beam momentum for a momentum transfer cutoff, $t_c = -0.4\,(\mathrm{BeV/c})^2$. $s^{1/2}$ is the total c.m. energy. The smooth curve is of the form $(1.4 \pm 1.8 + (4.5 \pm 1.5)\ln(s-1.4)$.

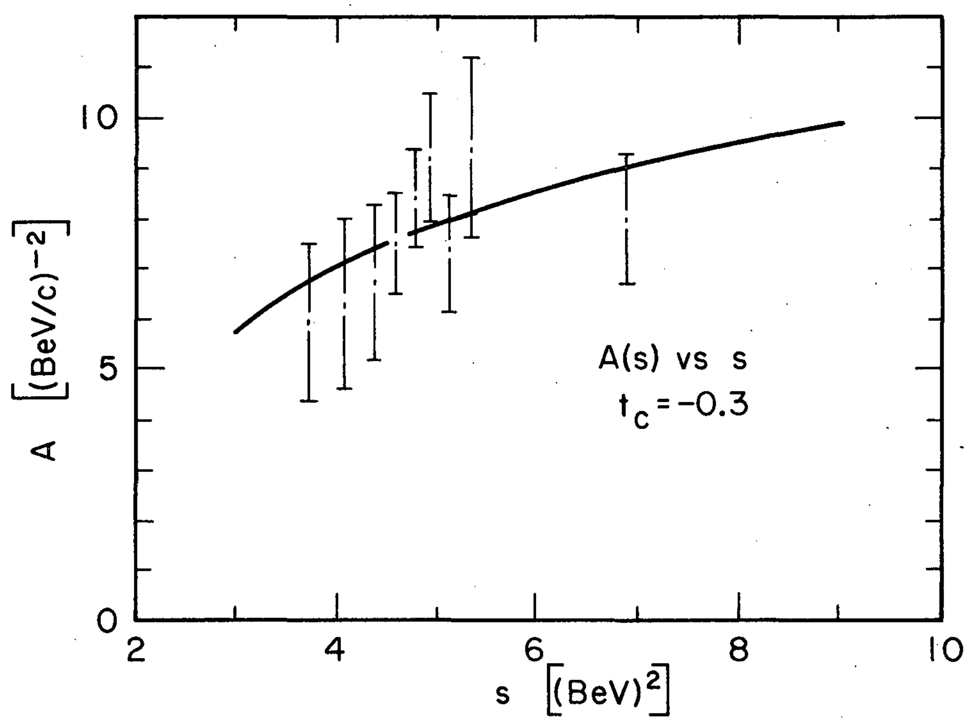

MU-34338

Fig. 24. Values of A vs beam momentum for $t_c = -0.3 (BeV/c)^2$. The smooth curve is of the form $(4.5 \pm 2.6) + (2.7 \pm 2.1) \ln(s - 1.4)$.

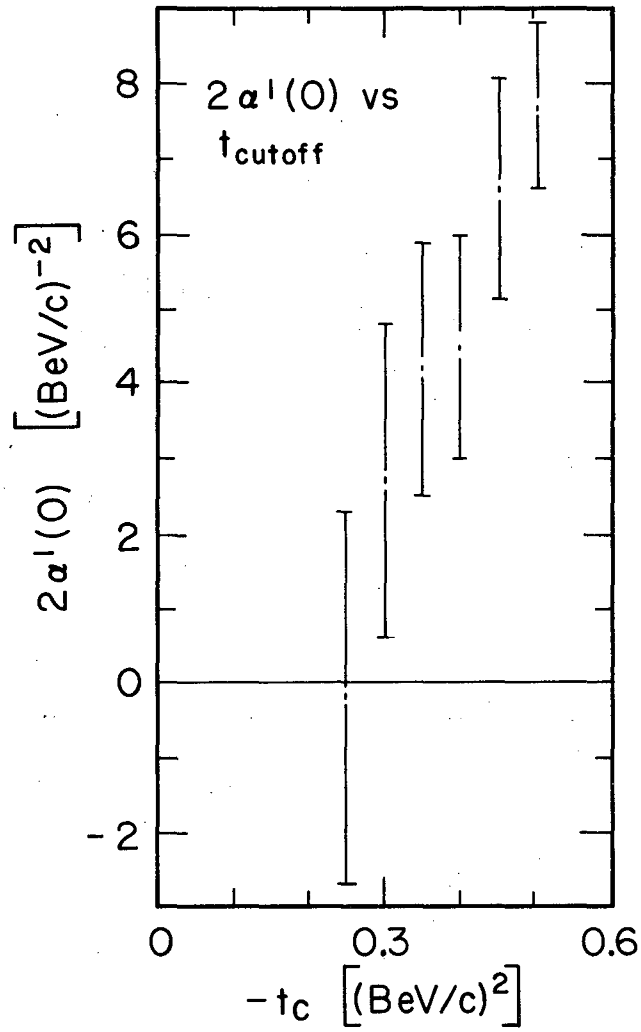

MU-34339

Fig. 25. Values of the slope of the K^* trajectory, $2\alpha'(0)$, vs momentum transfer cutoff.

ACKNOWLEDGMENTS

It is a pleasure to acknowledge the hospitality provided by Professor Luis Alvarez and members of his group. I have benefited from a year's collaboration with Professor Robert Tripp and Dr. Janos Kirz. This experiment would not have been possible without the efforts of many people. Professor Harold Ticho designed the original K beam. Dr. George Kalbfleisch wrote the heavy-duty data-analysis programs which are essential to projects of this size. Dr. Gerry Smith has participated in all but the very last stage of the experiment.

Dr. Jerry Anderson has always been willing to argue with me and has contributed many of the ideas contained in this work. Finally I wish to thank Professor Donald Miller for his sardonic encouragement throughout the entire period of my graduate education.

This work was done under the auspices of the U. S. Atomic Energy Commission.

REFERENCES

1. F. S. Crawford Jr., M. Cresti, M. L. Good, K. Gottstein, E. M. Lyman, F. T. Solmitz, M. L. Stevenson, and H. K. Ticho, in Proceedings of the 1958 Annual International Conference on High Energy Physics at CERN (CERN, Geneva, 1958), p. 323.
2. J. A. Anderson, F. S. Crawford, B. B. Crawford, R. L. Golden, L. J. Lloyd, G. W. Meisner, and R. L. Price, in Proceedings of the 1962 Annual International Conference on High Energy Physics at CERN (CERN, Geneva, 1962), p. 270.
3. L. Bertanza, P. L. Connolly, B. B. Culwick, F. R. Eisler, T. Morris, R. Palmer, A. Prodell, and N. P. Samios, Phys. Rev. Letters 8, 332 (1962).
4. F. Eisler, R. Plano, A. Prodell, N. Samios, M. Schwartz, J. Steinberger, P. Bassi, V. Borelli, G. Puppi, H. Tanaka, P. Waloschek, V. Zobaldi, M. Conversi, P. Franzini, I. Mannelli, R. Santangelo, and V. Silvestrini, Nuovo Cimento 10, 468 (1958).
5. J. L. Brown, D. A. Glaser, and M. L. Perl, Phys. Rev. 108, 1036 (1957).
6. Collaboration: Saclay, Orsay, Bari, and Bologne, in Proceedings of the Aix-en-Provence International Conference on Elementary Particles (Centre d'Etudes Nucléaires de Saclay, Seine et Oise, 1961), Vol. 1, p. 375.
7. R. K. Adair and L. B. Leipuner, Phys. Rev. 109, 1358 (1958).
8. F. S. Crawford Jr., R. L. Douglass, M. L. Good, G. R. Kalbfleisch, M. L. Stevenson, and H. K. Ticho, Phys. Rev. Letters 3, 394 (1959).
9. L. L. Yoder, C. T. Coffin, D. I. Meyer, and K. M. Terwilliger, Phys. Rev. 132, 1778 (1963).
10. Joseph Keren, Phys. Rev. 133, 13457 (1964).

11. J. A. Anderson, Strange Particle Production by 1170-MeV/c π^- Mesons in Hydrogen (Ph. D. Thesis), Lawrence Radiation Laboratory Report UCRL-10838, May 27, 1963 (unpublished).

12. R. D. Tripp, M. B. Watson, and M. Ferro-Luzzi, Phys. Rev. Letters 8, 175 (1962). A more extensive discussion is given in M. B. Watson, M. Ferro-Luzzi, and R. D. Tripp, Lawrence Radiation Laboratory Report UCRL-10542, January 15, 1963 (unpublished).

13. The assignment of appropriate levels for χ^2 cutoffs, is largely a question of taste. This has been expressed by J. P. Berge as "Low χ^2 is good, high χ^2 is bad."

14. We take $\tau_\Lambda = 2.59 \pm 0.07$, $\tau_K = 0.86 \pm 0.03$ (10^{-10}sec) as measured in this experiment, $\tau_\Sigma = 1.61 \pm 0.1$ as given in W. H. Barkas and A. H. Rosenfeld, Data for Elementary Particle Physics, Lawrence Radiation Laboratory Report UCRL-8030, Rev. April 1963 (unpublished).

15. For Σ^-, the arguments in the exponentials have to be changed to integrals over the path length to account for the track curvature and energy loss.

16. A. N. Diddens, E. W. Jenkins, T. F. Kycia, and K. F. Riley, Phys. Rev. Letters 10, 262 (1963).

17. The so-called standard error of the mean, $\sigma_{\overline{X}}$, of a sample of N measurements is $\sigma_{\overline{X}} \approx \sigma/\sqrt{N}$, where σ^2 is the variance of the sample. If the distribution is Poisson, then $\sigma \approx \sqrt{\overline{X}} = \sqrt{\sum_i N_i/N}$ and the fractional error is just $\sigma_{\overline{X}}/\overline{X} = 1/\sqrt{N_T}$, where N_T is the total number of events or tracks counted, just as expected. The distribution is not Poisson, so a nonuniform distribution of rolls scanned tends to emphasize fluctuations. The scan was actually done in bunches of neighboring rolls, which in one extreme case effectively reduced the number of measurements to the number of bunches (2).

18. A check scan for zero prongs using the same technique gives good agreement with the values obtained by Falk et al. in Proceedings of the Aix-en-Provence International Conference on Elementary Particles (Centre d'Etudes Nucléaires de Saclay Seine et Oise, 1961), Vol. 1, p. 50. The small-angle scattering inefficiency is estimated by assuming that the scanners miss all the events with a proton range $R < 1.5 \pm 1$ cm, and using the approximation for small angles $d\sigma/d\Omega = \sigma_o e^{-At}$, where $t^{1/2}$ is the momentum transfer, and $A = 7\ (\mathrm{BeV}/c)^{-2}$, as given by C. C. Ting, L. W. Jones, and M. L. Perl, Phys. Rev. Letters 9, 468 (1962).

19. In a fancy separation we would fit the missing-mass spectrum to a Gaussian for the K^0 peak plus an isotropic distribution for the Σ^0's. The area under the Gaussian would be taken as the estimate of the number of Λ's in a given histogram interval. See P. Bastien, K^--Proton Interactions near 760 MeV/c (Ph. D. Thesis), Lawrence Radiation Laboratory Report UCRL-10779, February 1963 (unpublished).

20. The cross section of reference 9 is not shown because of Yoder et al.'s ability to detect forward produced Λ's.

21. I use the notation N_I^*(mass) for the nucleon isobars where I = isotopic spin.

22. To gain statistics the number of beam momenta has been reduced to the three intervals (1450 to 1760), (1800 to 2000), and (2100 to 2200) MeV/c.

23. This diagram has a fairly extensive literature. See G. T. Hoff, Phys. Rev. 131, 1302 (1963) for a recent calculation and further references. See also reference 31.

24. With the scattering amplitude $M = f + i\,\sigma \cdot n g$ the angular distributions and polarization are invariant under the transformation $f \leftrightarrow g^*$. See R. H. Capps, Phys. Rev. 126, 1574 (1962).

25. A rose is a rose is a rose. The existence of these ambiguities has caused a certain amount of controversy in the past. See, for example, E. Segrè, in Proceedings of the 1962 Annual International Conference on High Energy Physics at CERN (CERN, (CERN, Geneva, 1962), p. 23, and R. Adair, ibid, p. 403.

26. P. Auvil and C. Lovelace, πp Phenomenology, 300-1300 MeV, Physics Department Imperial College, London, March 1964 (unpublished).

27. The only significant A_8 is at $P\pi = 2150$ MeV/c, where $A_8 = 14.4 \pm 5.5\,\mu b/sr$ (2.6 standard deviations).

28. For a simple derivation of barrier penetration factors see M. Gell-Mann and K. M. Watson, The Interactions Between π Mesons and Nucleons, in Annual Reviews of Nuclear Science (Annual Reviews Inc., Stanford, California, 1954), Vol. 4, p. 221. A complete discussion is given in J. M. Blatt and V. F. Weisskopf, Theoretical Nuclear Physics (John Wiley and Sons, New York, 1952), Chaps. VIII and X.

29. G. F. Chew and S. C. Frautschi, Phys. Rev. Letters 8, 41 (1962).

30. T. F. Kycia and K. F. Riley, Phys. Rev. Letters 10, 266 (1963).

31. William G. Wagner and David H. Sharp, M. Meson and a Generalization of the Pomeranchuk Relations, Phys. Rev. 128, 2899 (1962).

32. E. J. Squires, Complex Angular Momentum and Particle Physics (W. A. Benjamin, Inc., New York, 1963).

33. S. C. Frautschi, Regge Poles and S-Matrix Theory (W. A. Benjamin, Inc., New York, 1963).

34. R. Omnes and M. Froissart, Regge Poles and Mandelstam Theory (W. A. Benjamin, Inc., New York, 1963).

35. W. Kummer, Speculations on Experimental Consequences of Regge Poles, CERN 62-13, Theory Division, March 13, 1963 (unpublished).

36. C. E. Jones and J. A. Poirier, Basic Theory and Application of Regge Poles, Lawrence Radiation Laboratory Report UCRL-10677, February 8, 1963 (unpublished).

37. S. J. Lindenbaum, High Energy Scattering of $\pi^{\pm}$, p, $\bar{p}$ and $K^{\pm}$ by Protons, talk given at the International Conference on Nucleon Structure at Stanford, September, 1963 (unpublished report from Brookhaven National Laboratory). For published data see K. T. Foley, S. J. Lindenbaum, W. A. Love, S. Ozaki, J. J. Russell, and L. C. L. Yuan, Phys. Rev. Letters 10, 376 (1963) and 10, 543 (1963).

38. S. D. Drell, High Energy Physics, in Proceedings of the 1962 Annual International Conference on High Energy Physics at CERN CERN, Geneva, 1962), p. 900.

39. W. O. Lock, High Energy Nuclear Physics (Metheun and Co., Ltd. London, 1960), pp. 116-117.

40. Data from a subsequent run at $P\pi^{-} = 3200$ MeV/c $[s = 6.9(\text{BeV})^2]$ have been included in the presentation. The single K events have been excluded because of the poor resolution for forward-produced K^{0}'s.

41. For the equal-mass case, we have the expansion $P_{\alpha}(\cos\theta_t) \rightarrow (\cos\theta_t)^{\alpha} \approx (S - M^2)^{\alpha}$. Previous authors have taken $S >> M^2$. I have included the mass term as a perhaps fatuous correction.

42. These values are rather high. The slopes are expected to be of the order of $1(\text{BeV})^{-1}$. In p-p scattering $\alpha'(0)$ has been found to be $= 0.83 \pm 0.07$ (reference 34).

0 0 0 9 2 2 0 2 9 9 5

This report was prepared as an account of Government sponsored work. Neither the United States, nor the Commission, nor any person acting on behalf of the Commission:

A. Makes any warranty or representation, expressed or implied, with respect to the accuracy, completeness, or usefulness of the information contained in this report, or that the use of any information, apparatus, method, or process disclosed in this report may not infringe privately owned rights; or

B. Assumes any liabilities with respect to the use of, or for damages resulting from the use of any information, apparatus, method, or process disclosed in this report.

As used in the above, "person acting on behalf of the Commission" includes any employee or contractor of the Commission, or employee of such contractor, to the extent that such employee or contractor of the Commission, or employee of such contractor prepares, disseminates, or provides access to, any information pursuant to his employment or contract with the Commission, or his employment with such contractor.